remote sensing

MDPI

Review

Review of Remote Sensing Applications in Grassland Monitoring

Zhaobin Wang [1,2,*], Yikun Ma [1], Yaonan Zhang [2,3] and Jiali Shang [4]

[1] School of Information Science and Engineering, Lanzhou University, Lanzhou 730000, China; mayikun@lzu.edu.cn
[2] National Cryosphere Desert Data Center, Lanzhou 730000, China; yaonan@lzb.ac.cn
[3] Northwest Institute of Eco-Environment and Resources, Chinese Academy of Sciences, Lanzhou 730000, China
[4] Agriculture and Agri-Food Canada, 960 Carling Avenue, Ottawa, ON K1A 0C6, Canada; jiali.shang@agr.gc.ca
* Correspondence: zhaobin_wang@hotmail.com or wangzhb@lzu.edu.cn

Abstract: The application of remote sensing technology in grassland monitoring and management has been ongoing for decades. Compared with traditional ground measurements, remote sensing technology has the overall advantage of convenience, efficiency, and cost effectiveness, especially over large areas. This paper provides a comprehensive review of the latest remote sensing estimation methods for some critical grassland parameters, including above-ground biomass, primary productivity, fractional vegetation cover, and leaf area index. Then, the applications of remote sensing monitoring are also reviewed from the perspective of their use of these parameters and other remote sensing data. In detail, grassland degradation and grassland use monitoring are evaluated. In addition, disaster monitoring and carbon cycle monitoring are also included. Overall, most studies have used empirical models and statistical regression models, while the number of machine learning approaches has an increasing trend. In addition, some specialized methods, such as the light use efficiency approaches for primary productivity and the mixed pixel decomposition methods for vegetation coverage, have been widely used and improved. However, all the above methods have certain limitations. For future work, it is recommended that most applications should adopt the advanced estimation methods rather than simple statistical regression models. In particular, the potential of deep learning in processing high-dimensional data and fitting non-linear relationships should be further explored. Meanwhile, it is also important to explore the potential of some new vegetation indices based on the spectral characteristics of the specific grassland under study. Finally, the fusion of multi-source images should also be considered to address the deficiencies in information and resolution of remote sensing images acquired by a single sensor or satellite.

Keywords: grassland remote sensing; parameter estimation; land degradation monitoring; grassland use; disaster monitoring; carbon cycle

Citation: Wang, Z.; Ma, Y.; Zhang, Y.; Shang, J. Review of Remote Sensing Applications in Grassland Monitoring. *Remote Sens.* **2022**, *14*, 2903. https://doi.org/10.3390/rs14122903

Academic Editor: Eric Casella

Received: 28 March 2022
Accepted: 9 June 2022
Published: 17 June 2022

1. Introduction

Grassland, an important vegetation type in terrestrial ecosystems, is the most widely distributed form of land cover with abundant renewable natural resources [1]. It has many important ecological functions, such as sand fixation, water conservation, and diversity maintenance. It plays an essential role in livestock production, economy, and tourism [2], providing incomes for many people. On the one hand, grasslands are the main food sources of livestock products such as beef, lamb, and dairy. On the other hand, the natural scenery of grasslands and the historical relics of pastoralist peoples constitute the landscape resources that have important cultural and tourism values.

However, many grasslands have become significantly degraded in recent years due to human activities (pollution, over-grazing, and farmland reclamation) and extreme climate events (frost, rainstorm, and sandstorm), which have led to a decrease in soil moisture

and fertility, eventually leading to land desertification [3]. Thus, the conservation of ecosystems and the rational use of natural resources have become more and more critical in environmental decision making over the years. Grasslands are sensitive ecosystems where even slight changes in the surface can have a significant impact on the dynamic processes, not to mention the fact that they are often threatened by many natural hazards such as fire, drought, and insect damage. Therefore, the monitoring of both human activities and major disasters in grasslands is of great significance for grassland use management [4], disaster warning [5], post-disaster reconstruction [6], and sustainable development of grassland resources [7].

In general, accurate measurements of grassland biophysical and biochemical parameters are the basis of grassland monitoring. Traditional measurement methods rely mainly on ground measurements, also known as field surveys, which usually sample the measured area and select numerous plots to present the entire area. These plots can be directly used to generate accurately measured parameters or provide all kinds of precise data related to them. However, these methods are time-consuming and laborious, and they are only precise in small regions so that they are not suitable on regional and global scales.

Remote sensing technology has greatly advanced the operational monitoring of grasslands, which has rapidly replaced the traditional methods with significant advantages of convenience, efficiency, and reduced costs. In general, there are two types of optical remote sensing images mainly applied in this field: multispectral and hyperspectral images. Multispectral images are the most commonly used. In particular, multispectral images utilized in most studies are provided by the moderate-resolution imaging spectroradiometer (MODIS), which is a sensor on Terra and Aqua satellites. Both satellites are in sun-synchronous orbits so that they can provide daily images with a wide observation range, which allows researchers to easily estimate grassland parameters on regional and global scales. Although MODIS data have a fine temporal resolution, their low spatial resolution limits the accuracy and robustness of research results. Fortunately, with many advanced satellites being launched, more and more high-quality images are available. Apart from MODIS images, some other multispectral images, which are usually obtained from SPOT, Landsat, and Sentinel satellites [8,9] with hundreds of spectral bands, have also been widely adopted [10–12]. Meanwhile, hyperspectral images have also become popular recently [8,13,14]. In addition to optical satellites, some radar satellites such as the advanced land observing satellite (ALOS) and ENVISAT-1 satellites have been adopted in many studies. These satellites can provide synthetic aperture radar (SAR) images that are directly utilized for parameter estimation [15] and monitoring [16,17] or are added to models along with optical data to improve robustness [18]. In addition, radar satellites can also provide auxiliary information such as topographic data and soil indices to improve the accuracy of estimated results [19,20].

Apart from satellite images, a number of multispectral and hyperspectral sensors such as HyMap and compact airborne spectrographic imager can also be mounted on unmanned aerial vehicles (UAV) and airplanes to acquire near-surface imagery with high spatial resolution. These have been applied in some research recently [21–25]. Furthermore, some portable spectrometers such as Analytical Spectral Device (ASD) can work directly on the ground, producing ground images with super-high-spatial resolution that can be applied to study vegetation characteristics at fine scales (leaf and canopy levels) [26–29]. In some cases [6,30], these ground images serve as the reference to verify the robustness of satellite images. In addition, the light detection and ranging (LiDAR), a type of radar sensing, can be installed on the UAV or on the ground to provide supplementary information for parameter estimation [31,32].

Based on specific spectral bands of the above optical images, some vegetation indices have been developed. The normalized difference vegetation index (NDVI) and the enhanced vegetation index (EVI) have been widely used in most studies [33–36] due to their strong correlation with the growth status and spatial distribution density of plants. Huete et al. [37] demonstrated the high sensitivity of the NDVI and the EVI to spatio-temporal variation in

vegetation, land cover, and biophysical parameters. However, in some cases, the applicability of the NDVI may be challenged. As a result, some improved vegetation indices have been applied [26,38], such as the modified soil adjusted vegetation index (MSAVI) and the soil adjusted vegetation index (SAVI), which diminish the interference of noise and soil background faced by the original NDVI. In addition, for different research purposes, other indices such as the land surface water index (LSWI) and some red-edge indices have been fully utilized [39,40]. In some studies [41–43], researchers can even customize some new indices depending on the characteristics of grasslands under study. In [44], Xue and Su detailed the spectral characteristics of vegetation and summarized the development of over 100 vegetation indices and their specific applicability and representation under different conditions.

Furthermore, satellites can directly supply a number of products for atmospheric, terrestrial, and oceanic research. For grasslands, they can provide estimation products for temperature, surface albedo, leaf area index (LAI), etc. However, the accuracy of many estimation products is not robust in some cases. Taking some of the products from MODIS sensors as examples, Zhu et al. [45] reported a general underestimation in the MOD17A2 product that can provide an estimated parameter called gross primary productivity (GPP). Another product, MCD64A1, also has a significant underestimation of burned area that was demonstrated by [46]. Therefore, most current researchers prefer to estimate grassland parameters by establishing relationships between the highly relevant remote sensing indices and the actual values of these parameters obtained from ground measurements. To this end, all kinds of specific models and integrated frameworks have been proposed and developed based on the respective characteristics of different parameters. Various forms of statistical regression models and machine learning models have been widely used [47,48]. Meanwhile, some specialized methods have been developed such as the Carnegie–Ames–Stanford approach (CASA) model for primary productivity and the linear pixel dichotomy method for fractional vegetation cover (FVC). In addition, these estimated parameters have been adopted as the metrics of vegetation status in many practical applications such as grazing monitoring [49], burned area monitoring [6], and desertification monitoring [50].

Many recent studies have reviewed the use of optical imagery [51] and radar imagery [52] to vegetation monitoring and have demonstrated the great potential of remote sensing technology in some specific applications such as precision agriculture [53], forestry management [54], and carbon cycle monitoring [55]. Although there have also been a number of published reviews covering the applications of remote sensing images in grasslands [1,2,56–58], to our best knowledge, few of them focused on the relationship between key grassland parameters and remote sensing data. To this end, this paper presents a comprehensive review of the latest remote sensing estimation methods for some key grassland parameters and then reviews some specific monitoring applications from the perspective of the utilization of both these key parameters and remote sensing data (shown in Table 1). We first searched on the Web of Science with the keywords of "grassland", "remote sensing", and "estimat*", which yielded the results of thousands of papers. Based on the results, we found that more than half of these studies focused on the estimation of biomass and productivity. Meanwhile, there were also a number of studies involving vegetation coverage and biochemical parameters such as FVC, LAI, chlorophyll content, and water content. On this basis, we selected four representative parameters including above-ground biomass (AGB), primary productivity, FVC, and LAI in this paper to provide an overview of their latest estimation methods. Specifically, we further searched for their relevant publications from 2018 to now and chose highly representative work, which ultimately yielded 29 papers for AGB, 25 papers for primary productivity, 18 papers for FVC, and 10 papers for LAI. In addition, we also searched for four popular applications of remote sensing monitoring over the past decade, resulting in 21 papers related to grassland degradation, 27 papers revelant to grassland use monitoring, 53 papers associated with natural disasters, and 17 papers about carbon cycling.

Table 1. Topics reviewed in this article.

	Estimation Methods	Operational Applications
Review focuses	**Key parameters:** AGB Primary productivity FVC LAI **Methods:** Statistical regression Machine learning Light use efficiency Mixed pixel decomposition Radiative transfer models	**Specific applications:** Degradation monitoring Grassland use monitoring Disaster monitoring Carbon cycle monitoring

Overall, we obtained a total of 200 papers for our review. The structure of this paper is organized as follows. We first review the estimation methods in Section 2. Then, the applications of remote sensing monitoring are reviewed from the perspective of their use of remote sensing data in Section 3. We statistically analyze the different remote sensing sources utilized in these studies and analyze the characteristics of estimation methods and applications in Section 4. Based on the analysis, some main limitations faced by these studies and several suggestions for future work are presented in Section 4. Finally, Section 5 summarizes this article.

2. Parameter Estimation

2.1. AGB

AGB is the main parameter of grassland biomass, and its estimation is the focus of the grassland study with the largest number of publications. It is usually defined as the organic matter produced by the photosynthesis of grassland plants, which can be expressed as the dry weight of grassland plants in the above-ground part of a unit area. It is one of the significant indices of global carbon cycling, reflecting the carbon sink potential of grassland vegetation [47], and its changes directly reveal the degree of grassland growth and degradation, easily employed to monitor overgrazing [59].

The estimation models of AGB can be divided into parametric and non-parametric models. Specifically, parametric models mainly include linear [25], logarithmic [21], exponential [33], and other forms of functional models [60] that belong to statistical regression methods, while non-parametric models mainly involve support vector machine (SVM) [47], random forest (RF) [61], and artificial neural network (ANN) [62], which are primarily machine learning methods. In general, parametric regression models first select variables significantly related to AGB, after which a pre-assumed functional relationship between the variables and AGB is fitted by statistical data. Meanwhile, according to the number of variables, parametric regression models can be further classified as univariate and multivariate models. Except for the abovementioned parametric models that belong to univariate models, the multivariate linear regression (MLR) model is one of the most commonly used multivariate models in this field [9,18,32].

For the selection of variables, due to the significant correlation between vegetation height and biomass, many studies have focused on the inversion of vegetation height, which in turn can be linked to the AGB. These studies share significant methodological similarities in which 3D point cloud data used for inversion were generated from UAV images, while parametric regression models were developed for estimation. Zhang et al. [21] generated dense 3D point cloud data from UAV RGB images, and vegetation height was generated by calculating the distance between the point cloud data and corresponding ground meshes. The AGB was eventually estimated by a logarithmic regression model using the mean vegetation height, which achieved the coefficient of determination (R^2) of 0.89 between the estimated and measured AGB. Then, Grüner et al. [60] also produced 3D point clouds

and calculated mean vegetation height based on the difference between digital surface model data and digital elevation model (DEM) data. Then, the AGB was estimated by a reduced major axis regression model whose robustness was demonstrated even under extreme weather conditions ($R^2 = 0.72$). In addition, in [25,27], the mean vegetation height was also derived from 3D point cloud data, and both of them were utilized to developed linear models for AGB estimation.

Apart from the mean vegetation height, other forms of vegetation height derived from UAV or gound images were also utilized. In [63], the 90th percentile of vegetation height was derived from UAV images and was adopted for estimation in temperate grasslands by a linear model, but the results indicated that the model worked successfully only at the beginning of the growing season, while at other times, an MLR model combined with the NDVI was necessary. In [27], the grass volume was derived from UAV images, but its performance was worse than that of mean vegetation height derived from ground images. Then, Xu et al. [32] adopted ground-based LiDAR data to generate a 3D point cloud, which derived minimum vegetation height and FVC that were utilized to construct an MLR model with the best performance ($R^2 = 0.87$). Furthermore, Wijesingha et al. [31] chose the 75th percentile of vegetation height derived from UAV images or ground-based LiDAR data as the variable in a linear model. Their results showed that the performance based on UAV data was slightly worse than that of LiDAR data. However, these studies are overly dependent on vegetation height, which led to an inability to cope with grasslands made up of complex structures and vegetation. Shi et al. [22] derived the red-green-blue vegetation index (RGBVI) and the surface bare ratio from UAV RGB images and combined them with ground-measured grazing intensity to create a polynomial regression model achieving R^2 of 0.88. Nevertheless, the above studies should be combined with satellite data to further improve their performance.

Among various satellite data, most researchers preferred to directly select some vegetation indices highly correlated with vegetation growth and status. Therefore, the NDVI has always been popular in studies [9,38,64–66]. In addition, EVI, SAVI, and LSWI were utilized in some studies [18,26,39]. For example, Li et al. [39] estimated peak AGB of alpine grasslands by an EVI-based linear model, and they further focused on the temporal variability of precipitation on the AGB so that a new index was developed through the principal component analysis (PCA) and an MLR model to quantify this variability. Kong et al. [9] selected VI2 (normalization value of green peak reflectance and red valley reflectance) and the NDVI as driving variables through correlation analysis and developed an MLR model for alpine grasslands, gaining R^2 of 0.87. Wang et al. [18] developed an MLR model, which combined optical and radar data as variables. However, these above-vegetation indices are easily disturbed by soil background. On this basis, Ren et al. [26] introduced a negative soil adjustment factor into SAVI to remove the effect of soil background and estimated the AGB in desert grasslands through a linear model, which demonstrated that the performance of the improved SAVI far exceeded that of the NDVI. However, their experiments were conducted on the ground using ASD hyperspectral images alone, requiring further validation on satellite images. Wang et al. [38] modified several typical vegetation indices according to the changes of FVC in different phenological periods to eliminate the effect of soil background in semiarid grasslands and then compared them on different regression models, demonstrating the logarithmic model based on the modified NDVI achieved the best performance ($R^2 = 0.71$).

Apart from soil background, the low spatial and temporal resolution of some satellite images also limits the accuracy of estimation. To improve the temporal continuity of the estimation results, Clementini et al. [64] integrated NDVI data from SPOT, MODIS, and Landsat satellites to generate a long time series of the AGB for grazing grasslands using a power function regression model. Then, for the improvement of spatial resolution, Pang et al. [67] proposed a satellite-scale simulated spectra method, which scaled up ASD hyperspectral images to the satellite level with high spatial resolution by a mixed pixel decomposition model. Then, a multi-granularity spectral segmentation algorithm

was adopted to extract spectral segmentation features that were used in an MLR model, achieving R^2 of 0.95. Furthermore, to obtain NDVI data with both high temporal and spatial resolution, Zeng et al. [68] built a rule-based piecewise regression tree model to fuse MODIS and Landsat images and generated averaged the NDVI time series with 30m resolution that were finally employed in an exponential model to estimate the AGB. In addition, some other factors have also been studied. KarakoÇ et al. [66] investigated the spectral properties of grasslands at different altitudes and with different biomass densities in the Mediterranean region. The performance of linear and exponential models based on various forms of the NDVI and simple ratio (SR) were compared, which indicated that the spectral saturation effect due to high biomass densities severely degraded the estimation accuracy, while the selection of indices depending on the spectral characteristics of grasslands was more crucial than the choice of regression models. In addition, Braun et al. [15] explored the possibility of using satellite radar data alone. PCA was applied to integrate SAR data and passive brightness temperature data from radar satellites, which showed that the radar-based exponential regression model performed better in a savanna with low biomass but could not cope with high biomass, only achieving the R^2 of 0.52. Bao et al. [69] adopted the wavelet-PCA to fuse SAR images and multispectral images and estimated the AGB by a linear model using fused bands, which significantly outperformed the models based on vegetation indices or SAR images alone. Similarly, in [18], the results showed that the combination of SAR data could dramatically boost the model performance. Thus, the combination of optical and radar data is a feasible option for improvement.

However, the improvement of the above optimization strategies is limited. Parametric estimation models generally do not perform well, especially in the case of high spatial heterogeneity and complex grass species. Compared to parametric models, non-parametric models also require the selection of variables, but they can freely learn from statistical data without any pre-assumed functional relationships. John et al. [70] developed a rule-based Cubist model, which belongs to the regression tree approach in which driving variables mainly include vegetation indices, satellite products, topographic and climatic variables. Then, Yin et al. [71] adopted the consistent adjustment of the climatology to actual observations method to fill the temporal gaps in Landsat images, generating a series of high temporal resolution images that were subsequently utilized to train a Gaussian process regression model, which achieved a relatively high accuracy ($R^2 = 0.64$) compared to univariate regression models. Naidoo et al. [61] developed an RF model using various forms of the NDVI and SR and some spectral bands as variables. Although their best results were obtained by using only the WorldView data due to its higher spatial resolution, the Sentinel optical data could also achieve comparable performance when combined with their SAR data. Finally, Zheng et al. [72] combined vegetation indices, meteorological data, and topographical data to drive an RF model gaining the R^2 of 0.76.

Apart from the combination of satellite data, some recent studies have combined ground survey data and remote sensing data [47,73,74]. In detail, Lyu et al. [74] combined the NDVI and the EVI with meteorological and soil variables to construct an ANN model achieving superior performance ($R^2 = 0.91$). Meng et al. [47] compared various statistical regression models with machine learning models driven by six indices from both ground and satellite data. They verified that the RF model achieved the best results with R^2 of 0.78. Finally, Zhou et al. [73] combined ground data with the NDVI and selected seven indices to drive an RF model whose results were subsequently taken as the driving field for the simulations of high accuracy surface modeling, which not only achieved better results ($R^2 = 0.85$) than machine learning models but also accurately reproduced the spatial distribution characteristics of the AGB. In their further analysis, they concluded that warm and humid climates, overgrazing, and population growth are the main factors to drive the AGB changes.

In summary, Table 2 shows more details about the above methods. The R^2 values between the estimated and actual AGB have been extracted according to their best exper-

imental results, which can be used to evaluate the conformance between estimated and actual values.

Table 2. Detailed information on the involved estimation studies for the AGB.

Authors	Methods	Grassland Type	Remote Sensing Data	Data Source	R^2
Bao et al. [69]	linear regression	semiarid	fused spectral band	satellite	0.79
Li et al. [39]	linear regression	alpine	EVI	satellite	0.85
van der Merwe et al. [25]	linear regression	tallgrass prairie	vegetation height	UAV	0.91
Ren et al. [26]	linear regression	desert	SAVI	ground	0.64
Wijesingha et al. [31]	linear regression	typical	vegetation height	ground	0.61
Rueda-Ayala et al. [27]	linear regression	grazing	vegetation height	ground	0.88
Braun et al. [15]	exponential regression	low-biomass savanna	SAR	satellite	0.52
Zeng et al. [68]	exponential regression	alpine	NDVI	satellite	0.48
Zhang et al. [65]	exponential regression	typical	NDVI	satellite	0.64
Chu [33]	exponential regression	alpine, temperate	NDVI	satellite	0.84
Wang et al. [38]	logarithmic regression	semiarid	NDVI	satellite	0.71
Zhang et al. [21]	logarithmic regression	alpine, desert, salt marsh	vegetation height	UAV	0.89
Shi et al. [22]	polynomial regression	alpine	RGBVI, surface bare ratio	UAV	0.88
Grüner et al. [60]	reduced major axis regression	temperate	vegetation height	UAV	0.72
Kong et al. [9]	MLR	alpine	VI2, NDVI	satellite	0.87
Lussem et al. [63]	MLR	temperate	NDVI, vegetation height	UAV	0.87
Xu et al. [32]	MLR	typical, temperate	FVC, vegetation height	ground	0.84
Pang et al. [67]	MLR	temperate, desert	spectral features	ground	0.95
Yin et al. [71]	Gaussian process regression	alpine	spectral bands	satellite	0.64
John et al. [70]	rule-based Cubist model	alpine, typical, desert	vegetation indices	satellite	0.68
Naidoo et al. [61]	RF	marshy	spectral bands	satellite	0.64
Zhou et al. [73]	RF	alpine	vegetation indices, products	satellite	0.85
Meng et al. [47]	RF	alpine	vegetation indices, products	satellite	0.78
Lyu et al. [74]	ANN	typical	vegetation indices, products	satellite	0.91
Yang et al. [62]	ANN	alpine	vegetation indices, products	satellite	0.76
Zeng et al. [72]	ANN	semiarid	vegetation indices	satellite	0.76

2.2. Primary Productivity

The main parameters involved in this field are GPP and net primary productivity (NPP). GPP is generally defined as the amount of organic carbon fixed by photosynthesis in unit time by green plants, which is the biggest carbon flux of terrestrial ecosystems, while NPP is equal to GPP minus autotrophic respiration, which reflects the efficiency of plants in fixing and converting photosynthetic products and also determines the material and energy available to heterotrophic organisms. Therefore, the accurate estimates of GPP and NPP and the precise tracking of their spatial and temporal changes are the basis for understanding ecosystem dynamics and studying regional carbon uptake and cycling.

It is worth noting that traditional specialized estimation methods in this field mainly include the process-based biogeochemical approach and the light-use efficiency (LUE) approach. The process-based biogeochemical approach, mainly including the Biome-BGC model and the boreal ecosystem productivity simulator model, simulates the physiological processes in plants such as the photosynthesis and the decomposition of organic matter. The LUE approach is generally founded on the absorption and conversion of incident solar radiation by plants, including the vegetation photosynthesis model (VPM) and the CASA model. Recently, with the widespread use of remote sensing technology, most studies have combined remote sensing data with traditional methods for estimation and monitoring at large scales. Among these methods, the CASA model is the most popular and widely used [75–78]. Based on it, NPP can be estimated by:

$$NPP = \varepsilon \times APAR \quad (1)$$

where ε is the actual LUE and $APAR$ is the absorbed photosynthetically active radiation.

$$APAR = SOL \times FPAR \times 0.5 \quad (2)$$

where SOL is the total solar radiation, $FPAR$ is the fraction of photosynthetic active radiation absorbed by vegetation canopy, and the coefficient of 0.5 is the proportion of vegetation utilizing active incoming solar radiation, which is a frequently used empirical value.

$$\varepsilon = T_{\varepsilon 1} \times T_{\varepsilon 2} \times W_{\varepsilon} \times \varepsilon_{\max} \quad (3)$$

where $\varepsilon_{\max}$ is the ideal maximum LUE, $T_{\varepsilon 1}$ and $T_{\varepsilon 2}$ are the environmental stress coefficients of temperature, and W_{ε} is the environmental stress coefficients of water. It is worth noting that $T_{\varepsilon 1}$, $T_{\varepsilon 2}$, and W_{ε} reflect the restriction of LUE.

Some satellites can directly provide NPP and GPP products. For example, MOD17 is a set of NPP and GPP products provided by MODIS. Their estimation algorithms are based on the LUE approach. However, the reliability of MODIS GPP products is still a challenge, especially with extreme or highly variable climates and high levels of human activities. Zhu et al. [45] evaluated the performance and robustness of MODIS GPP products in tropical, temperate, and alpine grasslands, demonstrating the products generally underestimate the actual GPP by approximately 32%. They attributed this problem to the bias of $\varepsilon_{\max}$ and the uncertainty of $FPAR$. Ye et al. [34] applied a GLOPEM-CEVSA model that belongs to the LUE approach for NPP estimation and adopted a defoliation formulation model to calculate the carbon consumed by grazing. Their results showed that grazing would cause an underestimation of NPP by about 29% in semiarid and arid grasslands. Thus, rather than directly adopting satellite products, researchers prefer to develop specific models for the study area to obtain more robust estimates. These models mainly belong to the above approaches and require numerous parameters to drive and calibrate [79–83]. However, similar to the problems in [45], most parameters are uncertain and sparse and are difficult to obtain by same measuring methods.

On this basis, the combination of ground and remote sensing data is fully utilized in many studies to calibrate the process-based biogeochemical models and LUE models. Nanzad et al. [79] combined satellite products and meteorological data to drive a boreal ecosystem productivity simulator model. You et al. [80] introduced NDVI-driven phenological indices to improve the Biome–BGC model and obtained an increase of 0.08 in R^2 compared to the original model ($R^2 = 0.84$). Biudes et al. [81] adopted vegetation indices and products from MODIS data to drive multiple models for GPP estimates in tropical savanna, demonstrating the VPM model performed best. Irisarri et al. [82] also utilized the NDVI to drive a LUE method and quantified the effects of temperature, precipitation, and human activity on NPP in arid grasslands. Yu [83] developed a LUE–VPM model based on satellite products for GPP estimation in alpine grasslands, which achieved a large decrease of 36.21 in the root mean square error (RMSE) metric compared to MODIS GPP products.

Meanwhile, Zhao et al. [75] optimized a CASA model for NPP estimation in temperate grasslands, which simulated SOL based on meteorological data, estimated $FPAR$ based on the NDVI and the ratio vegetation index (RVI), and derived ε based on temperature and LSWI. Their results demonstrated that the optimized model outperformed MODIS NPP products with 0.06 improvement in R^2. Then, the CASA model was also improved by Luo et al. [77], who modified the calculation of W_{ε} by LSWI, achieving an increase of 0.04 in R^2 and a decrease of 0.11 in RMSE compared to original model. Zheng et al. [76] also constructed a CASA model, which estimated $FPAR$ based on the NDVI and proved a strong correlation between spring phenology and NPP in alpine grasslands. In addition, the NDVI time series were built by Blanco et al. [84] using MODIS data to estimate $FPAR$ by a linear model, and NPP was calculated by a LUE method. Gaffney et al. [85] constructed the NDVI time series with high spatial and temporal resolution by fusing Landsat and MODIS data to fit the $APAR$ for semiarid rangelands, and the above-ground NPP was estimated by a linear model similar to Equation (1). Their results pointed out the potential confounding effect of dead vegetation biomass on $APAR$, especially in grasslands with a long growing season. Similarly, Liu et al. [86] also fused Landsat and MODIS data to construct the NDVI time series for $FPAR$ estimates and then calculated $APAR$ according to Equation (2). They assumed that annual grassland production is equal to $APAR$ accumulated during the growing season and obtained R^2 of 0.83 on California grasslands. In addition, the selection of $\varepsilon_{\max}$ is also crucial for a CASA model; many studies usually just rely on an empirical value [76,77], which is not suitable for all grasslands. Thus, Jin et al. [78] modified the

calculation of ε_{max} based on the least error criterion between the estimated and ground-measured NPP and established the quadratic u-curve functions of ε_{max} for different types of grasslands, which achieved a boosting of 0.09 in R^2 compared to the original model based on empirical values.

There are also some studies that have developed statistical regression models such as linear [40,87], exponential [88,89], power function [48], and MLR [28,90]. Most of these studies focused on the selection of driving variables for their models. In [40], the performance of the red-edge and non-red-edge vegetation indices was compared, which showed that the red-edge chlorophyll index could improve GPP estimation at large scales. In [88], the performance of several vegetation indices was also contrasted, which indicated that MSAVI based on an exponential model worked best. Sakowska et al. [87] adopted various vegetation indices from satellites and airplanes with linear models to investigate the scale dependency of NPP estimation, which showed that the near-infrared difference index (NIDI) performed best, and they further proved the potential of Sentinel multispectral images for large-scale estimation. Matthew et al. [91] applied a piecewise function between the maximum NDVI and the NPP considering the asymptotic and saturated nature of the NDVI to estimate the long-term annual production in the Great Plains, achieving R^2 of 0.79. Cerasoli et al. [28] simulated satellite images from ASD hyperspectral images and constructed an MLR model for GPP estimation in the Mediterranean. Unlike previous studies that only focused on vegetation indices, spectral band was also considered in [28] and proved to be as essential as vegetation indices. Then, Xu et al. [90] constructed an MLR model based on phenological variables and the maximum of GPP, both of which were derived from the EVI and land surface temperature products. In addition, Dieguez et al. [92] applied a harmonic oscillation function based on the obtained maximum and minimum NPP data from satellite products to fit the NPP dynamic curve for Uruguayan grasslands considering the effects of climate and grazing. Meroni et al. [93] estimated GPP by the assimilation of MODIS NDVI into a crop growth model that was driven by meteorological variables. The results showed that the assimilation method outperformed MODIS products with a 0.14 improvement in R^2.

Table 3 lists more details of most studies mentioned above. The values of R^2 are from the best experimental results of the involved studies. In addition, it is necessary to take environmental and human factors into account if we want to obtain highly accurate estimates. Many of the above studies have focused on the spatial and temporal variation of primary productivity and exploring the factors that cause changes. Gómez et al. [94] adopted MODIS GPP products to quantify the contribution of climate factors, sunshine, and nitrogen deposition for GPP estimation in alpine grasslands using MLR models. The results demonstrated that precipitation and temperature were the first and second most important variables, while nitrogen deposition also had a significant impact. The results in [84] also demonstrated that the temporal variability of NPP could be largely explained by the precipitation during growing seasons. Many others studies have also pointed out that precipitation and temperature directly affect the distribution and accumulation of primary production [48,75,79,82,92,94]. Apart from climate factors, the impact of grazing [34,77,82], fertilization treatment [28], beginning of growing season [76], and grassland policies [48] were also investigated. In addition, the influence of dead vegetation biomass and below-ground biomass should also be considered, especially in grasslands with long growing seasons [85,95]. In [95], the significant underestimation of NPP using peak live biomass alone was experimentally demonstrated, particularly in tropical grasslands, due to the neglect of dead vegetation and below-ground biomass. Therefore, adding some appropriate variables to the estimation process, depending on the characteristics of the grassland under study, can help improve the accuracy of the results.

Table 3. Detailed information on the involved estimation studies for primary productivity.

Authors	Methods	Grassland Type	Remote Sensing Data	Data Source	R^2
Ye et al. [34]	GLOPEM-CEVSA	semiarid, arid	NDVI	satellite	0.80
You et al. [80]	Biome-BGC	alpine	NDVI	satellite	0.92
Liu et al. [86]	LUE	mixed	NDVI	satellite	0.83
Zhao et al. [75]	CASA	temperate	NDVI, RVI, LSWI	satellite	0.72
Jin et al. [78]	CASA	typical, desert	NDVI	satellite	0.57
Zheng et al. [76]	CASA	alpine	NDVI	satellite	0.79
Luo et al. [77]	CASA	alpine	EVI, LSWI	satellite	0.48
Lin et al. [40]	linear regression	typical	red-edge chlorophyll index	satellite	0.77
Sakowska et al. [87]	linear regression	alpine	NIDI	satellite	0.90
Li et al. [88]	exponential regression	typical, desert	MSAVI	satellite	0.72
Zheng et al. [48]	power function regression	typical, desert	NDVI	satellite	0.74
Dieguez et al. [92]	harmonic oscillation function	typical	NPP product	satellite	0.78
Matthew et al. [91]	piecewise regression	mixed	maximum NDVI	satellite	0.79
Cerasoli et al. [28]	MLR	typical	spectral bands, vegetation indices	ground, satellite	0.80
Xu et al. [90]	MLR	typical	EVI, land surface temperature	satellite	0.89
Gómez et al. [94]	MLR	alpine	GPP product	satellite	0.80
Meroni et al. [93]	assimilation	typical	NDVI	satellite	0.67

2.3. FVC

FVC is defined as the percentage of the vertical projection of green vegetation over the entire calculated area, which is the basic parameter for describing the characteristics of the grassland ecosystem and for obtaining the condition of grassland vegetation with its changes. Its accurate estimation is of great practical significance for regional grassland environment evaluation, management, and degradation monitoring.

The commonly used ground measurement methods of FVC for the accurate verification in most estimation methods are different from those of the previous parameters. Although sampling methods for ground measurements exist, the most commonly used method is the threshold-based photographic method that usually employs digital cameras or spectrometers to shoot the ground. Some studies focused on FVC estimation at near-surface and proved the validity of the photographic method [24,96,97]. In [24], the excess green index was calculated based on UAV RGB images for each pixel with a threshold to distinguish vegetation and non-vegetation pixels through an iterative algorithm. Then, the effect of the degree of vegetation fragmentation on the number of required sample images for validation was also investigated in [24]. Xu et al. [96] adopted ground-based RGB images, which set thresholds for the pixel difference values between different bands of RGB images to distinguish photosynthetic vegetation and senescent vegetation and then estimated the coverage. In addition, Kim et al. [97] also utilized ground-based RGB images but transformed them into three types of color spaces, and the histogram algorithm based on HIS color space achieved the best performance for arid and semiarid grasslands with R^2 of 0.97. However, their estimates failed on the regional scale with a very large RMSE, which might be due to the disturbance of both soil background and vegetation types and the mismatch of data at different scales.

For larger scale estimates, one of the most classic approaches is the mixed pixel decomposition method supported by the assumption that each pixel of an image may consist of multiple components such as bare ground, shrubs, and grassland. Thus, the information in the pixels can be decomposed to distinguish the different components, and FVC can be considered as the proportion of vegetation. Among various mixed pixel decomposition methods, the most classical and commonly used method is the linear pixel dichotomy, which supposes that the pixels are only composed of vegetation and bare soil components. Since the NDVI has proven to have a strong correlation with FVC, this method can be expressed as:

$$FVC = \frac{NDVI - NDVI_{soil}}{NDVI_{veg} - NDVI_{soil}} \times 100\% \quad (4)$$

where $NDVI_{veg}$ represents the NDVI value of the whole vegetation cover pixel, and $NDVI_{soil}$ is the NDVI value of the whole soil cover pixel. Generally, the values of $NDVI_{veg}$ and $NDVI_{soil}$ should be verified by ground measurements for different types of grasslands.

In addition, in specific studies, the NDVI can also be replaced by other vegetation indices or spectral bands that prove to be more closely related to FVC than the NDVI.

Zhang et al. [98] developed a linear pixel dichotomy model for the grasslands in Qaidam basin and compared its performance with that of an NDVI-based linear regression model, demonstrating that both had similar results in the evaluation of metrics but that the linear pixel dichotomy model suffered from a significant underestimation problem. Therefore, some studies attempted some other assumptions and utilized different remote sensing data. He et al. [99] assumed each pixel was composed of vegetation, bare soil, and water components, and they utilized the ground-based hyperspectral images to select the most relevant spectral bands to these components in semiarid grasslands, which achieved R^2 of 0.86. Recently, Vermeulen et al. [100] assumed that pixels were composed of grassy, woody, and bare soil components, and multiple vegetation indices and bands were combined to drive the model, which achieved the lowest RMSE value for FVC estimation of grassy components.

Meanwhile, models based on statistical regression or machine learning have also emerged in many studies. For statistical regression models, Zhang et al. [36] compared them with pixel decomposition methods and gradient difference methods for alpine, temperate, and desert grasslands, which showed that the logarithmic regression model obtained the best results on all types of grasslands, but all models were performed with low accuracy for alpine grasslands. Jansen et al. [101] studied the effect of different phenological periods on FVC estimation in grazing grasslands through linear regression models and found that the optimal driving variable of linear models was varied for each phenological period so that they further integrated the NDVI and set thresholds for it to automatically identify phenological periods and select variables. For machine learning methods, Meng et al. [102] evaluated the effectiveness of both statistical regression and machine learning methods in alpine grasslands, and all the machine learning methods were driven by both satellite and ground data. The results showed that the accuracy of machine learning models far exceeded that of statistical regression models, with the RF model achieving the best performance but suffering from poor stability. Then, Ge et al. [103] developed a SVM model for alpine grasslands, which significantly outperformed both linear pixel dichotomy models and statistical regression models in terms of R^2, RMSE, and F-test. Gao et al. [104] established an RF model by combining satellite and ground data as variables. Meanwhile, to validate the reliability of MODIS NDVI, a linear regression model was developed between MODIS NDVI and ground-based NDVI, and the NDVI finally adopted in the model was the mean value of them. Lin et al. [105] compared regression methods, linear pixel dichotomy method, and machine learning methods, which proved that the RF model outperformed others. The original RF model in [105] was driven only by vegetation indices achieving R^2 of 0.86, and the model was further optimized by adding spectral bands and topographical data to the driving variables, achieving a 0.06 improvement in R^2. Liu et al. [106] also adopted an RF model that was driven by vegetation indices, meteorological data, and topographical data, which obtained results with R^2 of 0.92 for grasslands.

Table 4 shows the details of the above methods with their best R^2 values. In addition, in terms of long-term monitoring, Yang et al. [107,108] focused on the spatiotemporal distribution of FVC in Chinese grasslands. In [107], they estimated and mapped the distribution for grasslands in western China over 300 years. They first simulated FVC without human disturbance, and then added this disturbance based on an historical cropland dataset and an empirical model built from modern land use data. Then, the same approach was adopted in [108] and was further combined with historical forest data to estimate FVC for grasslands in eastern China from 1700 to 2000. In addition, they also mapped its spatiotemporal changes and investigated the causes that mainly included population growth, agricultural expansion, and deforestation.

Table 4. Detailed information on the involved estimation studies for FVC.

Authors	Methods	Grassland Type	Remote Sensing Data	Data Source	R^2
Xu et al. [96]	threshold-based	semiarid	RGB images	ground	0.76
Kim et al. [97]	histogram	arid, semiarid	Hue channel of HIS color space	ground	0.94
Zhang et al. [98]	mixed pixel decomposition	typical	NDVI	satellite	0.98
He et al. [99]	mixed pixel decomposition	semiarid	red and near-infrared bands	satellite	0.86
Zhang et al. [36]	logarithmic regression	alpine, temperate, desert	NDVI	satellite	0.93
Jansen et al. [101]	linear regression	grazing	vegetation indices	satellite	0.81
Ge et al. [103]	SVM	alpine	vegetation indices, products	satellite	0.75
Meng et al. [102]	RF	alpine	vegetation indices, products	satellite	0.78
Gao et al. [104]	RF	alpine	vegetation indices, products	satellite, ground	0.88
Lin et al. [105]	RF	alpine	spectral bands, indices, products	satellite	0.92
Liu et al. [106]	RF	typical, desert	spectral bands, indices, products	satellite	0.92

Finally, apart from [96], some studies also concentrated on the FVC of senescent vegetation [109–111]. Chai et al. [109] simulated MODIS spectral bands from ground-based hyperspectral images and then calculated eight vegetation indices, demonstrating that a linear model driven by the dead fuel index (DFI) performed best with R^2 of 0.62. Then, Yu et al. [110] combined the DFI with the NDVI from MODIS in a linear mixed pixel decomposition model that supposes each pixel is composed of photosynthetic vegetation, senescent vegetation, and bare soil components. The results in [110] demonstrated that their proposed model achieved the best performance for FVC estimation of both photosynthetic vegetation and senescent vegetation at regional scales. Finally, based on their previous study [109], Chai et al. [111] directly derived DFI from MODIS data and introduced the NDVI to set thresholds for DFI to distinguish growing and non-growing periods of grasslands. They developed a DFI-based linear model for non-growing periods to estimate FVC of senescent vegetation at regional scales achieving R^2 of 0.6.

2.4. LAI

LAI is normally defined as half of the total green leaf area per unit surface area, which is closely related to plant photosynthesis, vegetation productivity, and ecosystem carbon accumulation. It is one of the key indices to reflect the growth status of grassland vegetation, as well as one of the most fundamental characteristic parameters in many ecosystem modeling processes.

Apart from direct destructive measurements, researchers can use ground-based optical sensors such as LAI-2200C and AccuPAR for non-destructive measurements. In addition, the radiative transfer models founded on physical principles are another approach for indirect measurements, which simulate radiative transfer processes in vegetation and describe canopy spectral changes as a function of canopy, leaf, and soil background characteristics. Among these models, the PROSAIL model, which is a combination of the SAIL canopy reflectance model and the PROSPECT leaf optical properties model, is the most popular and widely used. The construction of a PROSAIL model requires more than a dozen parameters including the LAI. Some of them are the physiological and biochemical parameters of the vegetation canopy and soil indices that can be obtained from satellite data and ground measurements, while other parameters usually do not have appropriate physical meanings and are hard to measure, so they are often assumed as empirical values based on prior knowledge in practice [112–114].

Many studies have focused on the radiative transfer models using both ground and satellite images. Punalekar et al. [114] adopted the PROSAIL model and estimated the LAI in grazing grasslands. Both ground and satellite images were adopted; the ground-based hyperspectral images were used to simulate multispectral images from satellites. The results showed that the simulated images could provide great accuracy at small scales ($R^2 = 0.87$), while the actual satellite images only offered relatively low accuracy ($R^2 = 0.76$) due to the overestimation problem in the case of high vegetation density. Pacheco-Labrador et al. [115] developed the soil-canopy observation photosynthesis and energy fluxes (SCOPE) model, which is the combination of radiative transfer model and soil-vegetation-atmosphere transfer models, and they introduced multiple constraints

to the model for different parameter estimation using ground images. As for the LAI, the model constrained by GPP and sun-induced fluorescence provided the best performance ($R^2 = 0.47$). Finally, Klingler et al. [116] developed PROSAIL models based on both simulated and actual satellite images, and the model based on actual satellite images provided the lowest RMSE value compared to the ground-based sensors. Pu et al. [112] applied a 3D radiative transfer model to investigate and quantify the uncertainty of MODIS LAI products caused by algorithms and input parameters, proving a significant underestimate problem of the products for grasslands with a low LAI.

Apart from the above methods, statistical regression and machine learning have also been applied in this field. Imran et al. [113] established a linear regression model to verify the strong correlation between ground measured LAI and the normalized difference index (NDI). In [113], ground-based hyperspectral images were adopted for the calculation of NDI and for the simulation of satellite-based NDI, and a PROSAIL model was also utilized to demonstrate that the grassland structural heterogeneity significantly affected the accuracy of the LAI estimation. Wang et al. [18] compared the performance of MLR, SVM, and RF models, which demonstrated that the MLR model driven by optical and radar data had the best performance with the lowest RMSE value, and the combination of radar data could further reduce RMSE value compared to using optical data only. For machine learning models, Karimi et al. [35] developed an RF model driven by the NDVI and meteorological data, which obtained highly accurate estimated results ($R^2 = 0.94$) in several grassland sites. Furthermore, in [117], the RF models driven by variables from different sources were compared, which showed that the model driven by optical variables could obtain a good accuracy ($R^2 = 0.63$) in semiarid grasslands, while the combination of SAR and DEM data could achieve a certain promotion ($R^2 = 0.68$). However, the promotion proved to be limited by the heterogeneity of studied grasslands. Schwieder et al. [118] also constructed an RF model driven by spectral bands and vegetation indices from satellites, and they compared the model with an improved PROSAIL model. The results showed that the RF model is slightly superior with an advantage of less than 0.01 for R^2.

In addition, Zhou et al. [119] constructed an ANN model driven by spectral bands from satellites and gained great performance for grasslands ($R^2 = 0.85$). Then, the model was combined with an assimilation model and MODIS LAI products to generate time-continuous LAI data with 30 m resolution. Recently, Danner et al. [120] combined the PROSAIL model with four machine learning models. Specifically, in [120], the PROSAIL model was adopted to simulate absent data from ground measurements so that a complete dataset could be provided for the training of machine learning methods. Then, these models were further trained with hyperspectral bands, and the results showed that although the ANN model outperformed others for the estimation of simulated LAI ($R^2 = 0.98$), its performance in real estimation did not significantly differ from that of other models. Finally, Table 5 shows the details of the above methods with their best R^2 values.

Table 5. Detailed information on the involved estimation studies for LAI.

Authors	Methods	Grassland Type	Remote Sensing Data	Data Source	R^2
Punalekar et al. [114]	PROSAIL	grazing	spectral bands	satellite, ground	0.76
Pacheco-Labrador et al. [115]	SCOPE	typical	spectral bands	ground	0.47
Imran et al. [113]	linear regression, PROSAIL	alpine	NDI	ground	0.8
Lu et al. [117]	RF	semiarid	vegetation indices, SAR	satellite	0.68
Karimi et al. [35]	RF	typical	NDVI	satellite	0.94
Schwieder et al. [118]	RF	typical	spectral bands, indices	satellite	0.79
Zhou et al. [119]	ANN, assimilation	typical	spectral bands	satellite	0.85
Danner et al. [120]	ANN, PROSAIL	typical	spectral bands	satellite, ground	0.98

3. Operational Applications

3.1. Grassland Degradation Monitoring

Grassland resources, as important land resources, have become significantly degraded in recent years due to human activities and extreme climates. Therefore, timely and accurate

monitoring of grassland changes and understanding the degree of degradation are the foundation of scientific grassland utilization [3]. In this, we review some representative work based on remote sensing in recent years.

First, some work directly made use of spectral bands and typical vegetation indices for monitoring. In 2012, Reiche et al. [121] classified the extent of grassland degradation in Inner Mongolia using a supervised maximum likelihood method based on SAVI and some specific bands from the Terra satellite. Then, to monitor the distribution of grasslands and farmlands, Li et al. [122] extracted the meaningful and homogeneous objects of the Mu Us desert from Landsat images using a multiresolution segmentation method, after which an assign class algorithm was employed to classify the objects based on RVI. In addition, a 3D convolution neural network for monitoring Inner Mongolia grasslands was established by Pi et al. [23], which only adopted UAV images with 231 hyperspectral bands as input. The experiments in [23] verified that the best results were obtained by using 44–166 bands.

Meanwhile, Lyu et al. [8] monitored the degradation from a new perspective of the vegetation species composition in the degraded grasslands. In detail, they first extracted spectral features from EO-1 hyperspectral images and reduced their dimensionality via PCA. Then, the multiple endmember spectral mixture analysis (MESMA) and the fully constrained least squares (FCLS) method were used to identify and classify the typical vegetation species in degraded grasslands. Similarly, Li et al. [123] captured ASD hyperspectral images to classify the dominant and degenerative grass species based on PCA, confidence interval mean difference (CIMD), and stepwise discriminant function. Recently, Pi et al. [124] constructed a 3D convolution neural network based on UAV hyperspectral images to classify the typical species in degraded grasslands, providing the quantitative metrics for degradation levels.

In other studies, some estimated parameters were utilized. In [125], FVC was fully utilized. A linear regression model between the NDVI and FVC was established to monitor the extent of desertification in Mongolian grasslands. Wiesmair et al. [126] also considered applying FVC to assess grassland degradation in the Georgian Caucasus. In [126], FVC was estimated by two RF models based on the NDVI and the MSAVI separately. The results showed that there was almost no gap in the mapping performance of the NDVI and the MSAVI for grassland degradation. Then, other types of grasslands parameters were also taken into account. Li et al. [127] established a remote sensing gradation system for grassland desertification in Ningxia, China. In [127], FVC and bare-sand ratio were both estimated by a mixed pixel decomposition model using Landsat images. Xu et al. [128] also estimated the bare-sand ratio based on the mixed pixel decomposition model and Landsat images, which were regarded as the main basis to monitor the variations of desertification in Tibet grasslands. Then, Wang et al. [129] built a CASA model to estimate NPP representing the vegetation status of grasslands in the Qinghai–Tibet Plateau, and they further quantified the impact of human activities and climate changes on desertification. Subsequently, Zhou et al. [50] considered NPP and FVC as monitoring indices of grassland degradation in China with reference to the GB 19377-2003 standard of China. In [50], NPP and FVC were estimated by CASA model and mixed pixel decomposition model, respectively. Finally, Zhumanova et al. [130] considered the influence of phenology. Specifically, they estimated FVC in various growing periods based on suitable univariate regression models, each of which adopted the MODIS NDVI in the corresponding period. Their results successfully demonstrated the distinctive manifestations of vegetation degradation in different phenological periods.

Furthermore, the joint use of remote sensing data and ground data further improved the accuracy of monitoring. Mansour et al. [10] proposed an RF method for mapping grassland degradation in the Cathedral Peak of South Africa, which first only used some specific spectral bands from SPOT satellites. However, they further found that the combination of three soil indices from ground observation in the model could achieve a nearly 13% accuracy improvement. Han et al. [131] adopted the multivariate hierarchical analysis based on both vegetation indices and ground data to classify the degradation on alpine

grasslands, and they further quantified the significance of each variable on the classification accuracy. Then, Lyu et al. [132] combined estimated parameters, NPP and FVC using MODIS NDVI, with three ground-based parameters, the AGB, soil bulk density, and soil organic matter to classify the degree of degradation in Inner Mongolia based on GB 19377-2003 standard. Yang et al. [133] introduced a grassland degradation index using six ground-based parameters to monitor grassland degradation in Shangri-La and applied RVI to fit this index by regression models, successfully verifying its accuracy for monitoring.

Finally, similarly to [133], some other new indices for monitoring were also created. A feature space proposed in [41] for monitoring desertification degree of semiarid grasslands was constructed by MSAVI and surface albedo, which generated a new index called the semiarid steppe desertification index. Zhang et al. [42] took the disturbance of climate fluctuations into account so that a new index, climate utilization efficiency (CUE), was constructed based on NPP to represent this disturbance. Then, CUE, NPP, FVC, and surface bareness were processed by PCA to further build a new comprehensive index for monitoring the grassland degradation in the Three-River Source Region of China. Guo et al. [134] combined an albedo–normalized difference vegetation index and MSAVI from Landsat images to create an index called the desertification monitoring index and monitored the desertification in the Naiman Banner based on linear regression models. Qian et al. [135] established a comprehensive index called the alpine grassland desertification index for monitoring the alpine grasslands. The index was built from AGB, FVC, and soil moisture, all of which were estimated from Landsat and MODIS images.

In conclusion, Table 6 lists more details about these studies. It can be seen that nearly half of the studies adopted the estimated parameters to replace the ground measurements. Among the estimated parameters, NPP and FVC are frequently adopted, and in most cases, they are estimated based on remote sensing. For their estimation models, the FVC in most studies is estimated by the mixed pixel decomposition model according to Equation (4), while NPP in all is estimated based on a CASA model. In addition, the number of studies using hyperspectral images is significantly less than that of the multispectral.

Table 6. Detailed information on the involved monitoring studies for grassland degradation.

Authors	Monitoring Methods	Estimated Parameters	Estimation Models	Remote Sensing Data
Li et al. [127]	decision-tree	FVC, bare-sand ratio	both: mixed pixel decomposition	multispectral bands
Zhou et al. [50]	threshold-based	NPP, FVC	NPP: CASA, FVC: mixed pixel decomposition	NDVI
Zhang et al. [42]	PCA, threshold-based	NPP, FVC, surface bareness	NPP: CASA, Others: mixed pixel decomposition	NDVI, soil temperature, multispectral bands
Lyu et al. [132]	constraint line method	NPP, FVC	NPP: CASA, FVC: mixed pixel decomposition	NDVI, EVI,DEM
Qian et al. [135]	geographical detector, threshold-based	AGB, FVC, soil moisture	AGB: logarithmic regression, FVC: mixed pixel decomposition, soil moisture: exponential regression	vegetation indices, products
Wiesmair et al. [126]	threshold-based	FVC	RF	NDVI, MSAVI
Sternberg et al. [125]	threshold-based	FVC	linear regression	NDVI
Wang et al. [129]	threshold-based	NPP	CASA	NDVI, LAI product
Zhumanova et al. [130]	threshold-based	FVC	univariate regression	NDVI
Xu et al. [128]	threshold-based	bare-sand ratio	mixed pixel decomposition	multispectral bands
Reiche et al. [121]	supervised maximum-likelihood	/	/	vegetation indices
Mansour et al. [10]	RF	/	/	multispectral bands
Li et al. [122]	multiresolution segmentation	/	/	multispectral bands
Wu et al. [41]	feature space	/	/	vegetation indices
Yang et al. [133]	multivariate statistical analysis	/	/	vegetation indices
Lyu et al. [8]	MESMA, FCLS	/	/	hyperspectral bands
Pi et al. [23]	convolution neural network	/	/	hyperspectral bands
Guo et al. [134]	linear regression, feature space	/	/	albedo index, MSAVI
Han et al. [131]	multivariate hierarchical analysis	/	/	vegetation indices, products
Pi et al. [124]	3D convolution neural network	/	/	hyperspectral bands
Li et al. [123]	CIMD, stepwise discriminant function	/	/	hyperspectral bands

3.2. Grassland Use Monitoring

As one of the terrestrial resources with high production value, the main uses of grasslands are grazing and mowing. However, overgrazing and over mowing can seriously disrupt the balance of grassland ecosystems, leading to a decline in ecosystem biodiversity

and even causing desertification. In recent years, the conservation and wise use of ecosystems have become increasingly important in environmental decision making. Many studies have shown that moderate grazing can effectively promote grassland productivity and improve the maintenance of biodiversity [4,59,136]. Thus, the economic needs of humans and the biodiversity of grasslands need to be balanced. For this purpose, the monitoring and management of grassland use are necessary, which implies the need for obtaining accurate related data and parameters at large scales. It also means that remote sensing data can fully explore its potential to provide effective reference and assistance for policy making. Here, the studies focused on monitoring the intensity of grazing and mowing are reviewed.

3.2.1. Grazing Monitoring

Grazing intensity (GI) is generally defined as the number of grazing animals per hectare of grassland. Since some biophysical parameters such as AGB, FVC, and LAI proved to have a strong correlation with GI, most studies in this field have tended to select one of these parameters to demonstrate the same correlation using ground measurements at a small field scale. Then, the ground-measured parameter was replaced by its estimated one based on remote sensing data to monitor at a larger scale.

First, many studies directly utilized the AGB as the metric to monitor grazing. Li et al. [137] applied the AGB to classify different GI based on thresholds, in which the one-way analysis of variance (ANOVA) and the frequency histograms from sample plots were utilized to determine the thresholds, and a three-layer ANN was adopted to estimate the AGB. Then, Xu et al. [59] also demonstrated the significant linear correlation between ground-measured AGB and GI in temperate meadow grasslands and used the HJ-1 NDVI to estimate the AGB for monitoring. Similarly, Ma et al. [136] adopted ground-measured AGB in meadow and semiarid grasslands, and they established a linear model to estimate the AGB by MODIS NDVI and a power function model to estimate GI. Their results showed an increasing trend of the AGB with increasing GI under moderate grazing pressure, which proved moderate grazing could effectively promote grassland productivity.

Meanwhile, other parameters were also adopted. Hall et al. [138] classified grazed and ungrazed areas by an object-based approach that simultaneously considered the spatial adjacency and spectral similarity of the pixels of QuickBird images. The performance of various indices was further validated in [138], and an SR index was chosen to build a linear model to estimate vegetation height that was adopted as the basis of GI. Then, Yang et al. [139] investigated the response of grassland biophysical parameters and vegetation indices to the GI of mixed grasslands. Their results showed that the vegetation height and the ratio of photosynthetically active vegetation cover to non-photosynthetically active vegetation cover (PV/NPV) could successfully identify different levels of GI. These two variables were estimated by MLR models where the modified triangular vegetation index 1 (MTVI1) and SAVI were adopted for PV/NPV and the plant senescence reflectance index (PSRI) and the normalized canopy index (NCI) were used for vegetation height. Then, in [140], the LAI was adopted as the basis, and a grazing-led exponential growth function was built for the LAI to monitor GI. Apart from the above studies, some studies also utilized multiple parameters. Feng and Zhao [141] built the CENTURY model, an ecosystem analysis tool that can assess climate change and human disturbance, monitoring GI in Inner Mongolia grasslands. The CENTURY model requires temperature, precipitation, soil water content (SWC), AGB, and FVC as input. In [141], among these variables, SWC was estimated by a thermal inertia model, while the AGB was estimated by first calculating the LAI through a GO-RT reflectance model and then linking the AGB and the LAI by a logarithmic regression model. Finally, Jansen et al. [142] selected vegetation structure, foliar cover, and the AGB as the key indices to assess GI, and all the parameters were estimated by MLR models.

In terms of the direct utilization of remote sensing data, Junges et al. [4] directly utilized the MODIS NDVI and the EVI time series to calculate their seasonal averages and

then plotted the average curves to analyze the characteristics under different GI levels and set thresholds to distinguish them. The results showed that the EVI was suitable for all seasons, while the NDVI could only work for spring and winter seasons. In addition, it is worth noting that the average values of the NDVI and the EVI under moderate GI condition were highest. This phenomenon had also been confirmed by the above studies [59,136]. Then, to detect grazing activities, Awuah et al. [49] adopted WorldView images to construct multiple machine learning models, including SVM, RF, classification and regression trees (CART), and multilayer perceptron (MLP), to map the distribution of grazing lawns in Southern African savannas. The results showed that the classification accuracy produced by models other than CART was comparable. In addition, Li et al. [143] designed a new index called the grazing intensity index using MODIS data to quantify the GI. The index was defined as the ratio of accumulated change in the NDVI over a continuous period relative to local grassland background, which was linked to GI by a linear regression model. However, due to the limitations of the NDVI, the GII could only be applied to the growth period.

Then, in canopy spectral measurements, Sha et al. [144] investigated the relationship between different GI in Inner Mongolia grasslands and eight vegetation indices derived from ground-based hyperspectral images. The results showed that each index was significantly negatively correlated with GI, and photochemical reflectance index (PRI), broad-band NDVI, and narrow-band NDVI were sensitive to GI. Then, Lei et al. [145] adopted UAV images and kernel density estimation (KDE) algorithm to constructed the GI index at field scale. This index was further combined with Sentinel NDVI to train an RF model to generate the regional GI. These studies using near-surface data also took full advantage of the significant relevance of the NDVI to vegetation status. However, the NDVI is not sensitive to the changes of green vegetation in some cases, especially in arid or semiarid grassland ecosystems due to its vulnerability to soil and dead plants. Therefore, Gimenez et al. [146] combined a normalized red-edge vegetation index (NREVI) with its coefficient of variation from RapidEye images and then used the K-means algorithm to classify the GI. Yang et al. [30] adopted the NCI calculated by Landsat images to eliminate disturbance from dead plants and analyze the effects of light on moderate grazing on mixed grassland production, which constructed a linear regression model between total biomass and NCI. Franke et al. [147] combined the NDVI and the NREVI with mean absolute spectral dynamic (MASD) to classify the GI. In their experiments, the classification methods based on decision-tree and context approaches were compared. Although the results show a higher accuracy, the decision-tree method suffered from an overfitting problem.

In addition, Li et al. [148] used vegetation indices from EO-1 hyperspectral images, but they developed an auxiliary spectral index named GMI to fit temporal changes of GI, which was combined with the AGB estimated by a linear model using a mixed index composed of the red-edge index (REI) and the cellulose absorption index (CAI). Different levels of GI were classified based on the threshold approach. Zheng et al. [149] exploited the characteristic of the red-edge position (REP) that the position would shift when exposed to vegetation stress to detect GI by a linear model between the shift and stocking rate. They experimentally demonstrated that grazing could lead to a shift of the REP toward short wavelengths, and the amplitude of the shift was highly related to stocking rate. However, these conclusions had to be further verified by satellite images. Finally, Dara et al. [150] also created a new index called grazing probability based on an RF model with 27 remote sensing indices as the inputs, and this index was successfully applied to classify the grazing pressure on the grasslands of Kazakhstan.

In conclusion, Table 7 shows more details about these studies. It can be seen that the AGB is the most frequently adopted parameter in these studies. More specifically, most of the AGB estimation models are based on statistical regression; only one model was based on ANN. In addition, most studies have focused on applying linear regression models to fit GI. Then, they detected different intensities of grassland use based on thresholds, while a few studies adopted machine learning models to classify different GI.

Table 7. Detailed information on the involved monitoring studies for grazing intensity.

Authors	Monitoring Methods	Estimated Parameters	Estimation Models	Remote Sensing Data
Li et al. [137]	threshold-based	AGB	ANN	multispectral bands
Xu et al. [59]	linear regression	AGB	linear regression	NDVI
Ma et al. [136]	power regression	AGB	linear regression	NDVI
Li et al. [148]	threshold-based	AGB	linear regression	REI, CAI
Yang et al. [30]	ANOVA, dynamic analysis	total biomass	linear regression	NCI
Hall et al. [138]	object-based	vegetation height	linear regression	SR, multispectral bands
Yang et al. [139]	linear regression	PV/NPV, vegetation height	MLR	MTVI1, SAVI, PRSI, NCI
Jansen et al. [142]	linear regression	AGB, foliar cover	MLR	vegetation indices
Feng and Zhao [141]	CENTURY model	AGB, SWC, LAI	AGB: logarithmic regression, SWC: thermal inertia model, LAI: GO-RT reflectance model	multispectral bands
Junges et al. [4]	linear regression	/	/	NDVI, EVI
Li et al. [143]	linear regression	/	/	NDVI
Sha et al. [144]	linear mixed model	/	/	vegetation indices
Zheng et al. [149]	linear regression	/	/	REP
Gimenez et al. [146]	K-means	/	/	NREVI
Franke et al. [147]	decision-tree, context approach	/	/	NDVI, MASD, NREVI
Yu et al. [140]	grazing-led exponential function	/	/	LAI product, land use data
Awuah et al. [49]	SVM, RF, MLP, CART	/	/	multispectral bands
Dara et al. [150]	RF	/	/	vegetation indices
Lei et al. [145]	RF, KDE	/	/	multispectral bands, vegetation indices

3.2.2. Mowing Monitoring

Another form of grassland use is fodder production, which requires mowing and processing the grass into silage or hay. The frequency and timing of mowing are influential characteristics of grassland use and can also be used to indicate the degree of grassland use intensity. However, the monitoring of mowing is somewhat different from that of grazing. On the one hand, the quality and production of grass are closely related to grassland phenology such as growing, flowering, and maturation periods. Herders generally choose the appropriate time to mow according to the type of sheep and cattle they feed. On the other hand, the duration of the mowing event is very short so that it requires remote sensing images with higher temporal frequency for monitoring.

Compared with grazing, fewer studies have been conducted for mowing monitoring. In 2014, Dusseux et al. [151] experimentally demonstrated the effectiveness of the LAI time series for monitoring grazing and mowing at a small scale, which estimated the LAI by the PROSPECT model and used the K-Nearest Neighbor algorithm to detect and map the distribution of grazing and mowing. Then, Asam et al. [152] investigated the performance of the LAI time series at a larger regional scale, which also utilized the PROSAIL model to produce the LAI time series from RapidEye data. In their method, the area under the time series and the mean absolute dynamic of the time series were calculated and then served as variables to drive a decision-tree model for the classification of grassland use intensities based on mowing frequency. Meanwhile, the the NDVI time series were directly utilized in [11,153–155]. Estel et al. [153] employed the NDVI time series from MODIS and applied a spline-fitting algorithm to detect the troughs of the time series. A threshold was used to determine the occurrence of mowing. However, the low spatial resolution of MODIS images affected the accuracy and reliability of their results, which highlighted the significance of high-resolution remote sensing images for mowing monitoring. Thus, Kolecka et al. [11] constructed the NDVI time series from Sentinel image;, they monitored mowing frequency by extracting mutations of time series based on empirical thresholds and took full account of the effect of the time interval before and after mutations. In their experiments, the effect of cloud cover leading to a reduction in the number of available images was also investigated; it showed that cloud cover could cause a significant overestimation of mowing frequency, and more accurate monitoring required denser time series. Griffiths et al. [154] applied a best-pixel scoring algorithm [156] to synthesize Sentinel and Landsat images to generate denser high-resolution images with 10-day intervals. Based on the synthesized images, the NDVI time series were also calculated and then were compared to the ideal NDVI time series without mowing where the residuals between the two were measured to identify potential mowing points. However, the results showed that the method failed to remove the effects of grazing and monitor the areas that experienced only one mowing.

Stumpf et al. [155] employed the NDVI to represent the AGB and also generated the NDVI time series from Landsat images. In their approach, the effects of grazing and mowing could be distinguished by setting a threshold for changes in the NDVI at adjacent time points and recording all the changes. The results indicated that for grazing areas, the sum of recorded changes was lower, and the NDVI series showed a gradual trend, while for mowing areas, the sum was higher, and the series showed some abrupt changes.

In addition, the potential of radar data was also exploited in [16,17]. There were several similarities between the two studies. In detail, they adopted the repeat-pass SAR interferometry and selected X-band for their studies. Both of the experiments proved that the interferometric coherence of SAR images had a strong correlation with vegetation height and biomass and that the combination of interferometric coherence and backscattering coefficient of SAR images had the potential to detect mowing events. However, the ability to detect mowing still needs further experimental validation and considers various interference factors, especially in [16], which demonstrated that wind can significantly affect vegetation height leading to the uncertainty of detection.

In summary, all studies in this field shared a same strategy, i.e., the growth state of the vegetation is simulated by the time series of some indices in which some abrupt changes that cannot be explained under normal growth state are marked and are further analyzed for detecting the real mowing events. Table 8 shows the details about these studies.

Table 8. Detailed information on the involved monitoring studies for mowing events.

Authors	Monitoring Methods	Parameters	Estimation Models	Remote Sesning Data
Dusseux et al. [151]	K-Nearest Neighbor	LAI	PROSAIL	satellite products
Asam et al. [152]	decision-tree	LAI	PROSAIL	satellite products
Estel et al. [153]	threshold-based	/	/	NDVI
Kolecka et al. [11]	threshold-based	/	/	NDVI
Griffiths et al. [154]	threshold-based	/	/	NDVI
Stumpf et al. [155]	K-means	/	/	NDVI
Ali et al. [16]	correlation analysis	/	/	X-band of SAR images
Zalite et al. [16]	correlation analysis	/	/	X-band of SAR images

3.3. Disaster Monitoring and Impact Analysis

3.3.1. Fire

Fire is one of the major disasters and threats to grassland ecosystems; it has an important impact on grassland ecological functions and species composition, which may be positive or negative. On the one hand, fire is a process of natural selection in which species that are adapted or resistant to fire will survive and recover quickly, becoming the dominant species of the ecosystem. On the other hand, extreme fires can cause unrecoverable damage under natural conditions, leading to the degradation of grasslands. Thus, effective fire warning and assessment can contribute to the reduction of fire frequency and damage and to post-disaster management. Recently, there have been many studies on the use of remote sensing for fire, which can be divided into the following aspects: risk assessment, dynamic monitoring, and impact analysis.

First, for risk assessment, Zhang et al. [5] transformed MODIS historical fire data from the point form to the continuous surface with kernel density estimation, and the fire risk zones were directly mapped based on the regional density averages. Apart from it, most studies mainly focused on some indices related to fire, and the accuracy of these indices seriously affects the reliability. At the beginning, the degree of grassland curing, which is defined as the proportion of senescent plants, is a critical parameter for fire research. Martin et al. [157] compared the performance of different indices from MODIS data on an MLR model for estimating the curing degree, which proved that the combination of the NDVI and the global vegetation monitoring index (GVMI) achieved the best performance. Due to the general underestimation and overestimation of MODIS indices in [157], the model was adjusted to achieve some improvement but was still limited by the low resolution of images. Chaivaranont et al. [158] also used MODIS data and established an MLR model similar to [157], but they replaced GVMI with the vegetation optical depth (VOD)and achieved comparable performance. Furthermore,

to break the limitations of MODIS images, Li [159] adopted finer Landsat images of the Greater Melbourne region and calculated the NDVI and global vegetation moisture index (GVMTI) forming an MLR model to estimate curing degree, achieving comparable accuracy to ground measurements. Recently, Li [160] further investigated the differences between Landsat, MODIS, and Sentinel images with different spatial resolutions in the inversion of curing degree so that recommended images for future studies were given based on their characteristics of research environment.

Apart from curing degree, the total organic matter available for ignition and combustion is another inescapable parameter in fire research, which is commonly defined as fuel in many studies. In 2012, Wang et al. [161] proposed a fire danger index based on the analytical hierarchy process and five estimated parameters, including curing degree and fuel weight, which was derived from Landsat images. Then, Bian et al. [162] created a grassland fire risk index that combined fuel, fire climate, accessibility, human–social factors, and topography data into an MLR model in which the NDVI was applied to represent the annual continuity of grassland fuels. In their experiments, the proposed index was used for the classification and mapping of fire risk in Inner Mongolia grasslands. Furthermore, Sesnie et al. [163] utilized 27 vegetation indices with topographic data and the coverage of different plant species to drive an RF model that estimated the fuel biomass in semiarid grasslands. The results indicated that the improvement of model accuracy required remote sensing data with higher temporal resolution. In addition, Jurdao et al. [164] focused on the live fuel moisture content (LFMC), which established an MLR model to estimate the LFMC and then generated the probability of fire for risk assessment based on another MLR model. Then, Arganara et al. [165] built a linear model between LFMC and EVI. They linked LFMC to the fire risk and generated a fire danger map in Argentina. Furthermore, a PROSAIL model was applied for LFMC inversion [166,167]. In [166], LFMC was associated with the grassland fire events through an MLR model and several thresholds, demonstrating a marked relationship between the pre-fire LFMC and fire events. Similarly, Yebra et al. [167] also built an MLR model based on various forms of LFMC to estimate the flammability of fuel that achieved a certain capability of fire prediction in Australia.

Table 9 statistics show the estimation methods of the above parameters as well as the remote sensing data utilized in the models. It can be seen that curing degree in all cases is estimated by an MLR model, and the NDVI is the most effective driving variable of the model. As for fuel biomass, the NDVI also plays an essential role in the estimation, and the PROSAIL model has been applied in LFMC estimation.

Table 9. The estimated parameters and their estimation models in the studies of fire risk assessment.

Authors	Estimated Parameters	Estimation Models	Remote Sesning Data
Martin et al. [157]	curing degree	MLR	NDVI,GVMI
Chaivaranont et al. [158]	curing degree	MLR	NDVI,VOD
Li [159]	curing degree	MLR	NDVI, GVMTI
Li [160]	curing degree	MLR	NDVI, GVMTI
Bian et al. [162]	fuel biomass	NDVI average curve	NDVI
Sesnie et al. [163]	fuel biomass	RF	vegetation indices
Wang et al. [161]	fuel biomass	linear regression	NDVI
Jurdao et al. [164]	LFMC	MLR	NDVI, surface temperature
Arganara et al. [165]	LFMC	linear regression	EVI
Luo et al. [166]	LFMC	PROSAIL	satellite products
Yebra et al. [167]	LFMC	PROSAIL	satellite products

Second, for dynamic monitoring, the effective and accurate monitoring of a burned area can assist in damage assessment, understanding the extent of ecological changes caused by the fire, and making restoration policies. In 2010, Dubinin et al. [168] performed a long time series of burned area reconstruction in the southern Russian arid grasslands by the NDVI and a decision-tree model. They estimated the annual burned area from 1985 to 2007, which was one of the longest time series of the burned area obtained by remote sensing. Then, Pereira et al. [169] directly segmented the burning area from the Landsat image through an object-based image segmentation algorithm and mapped the fire frequency in the Cerrado Savanna. Apart from them, many studies monitored the burning

area through grassland parameters and vegetation indices. Cao et al. [170] established an MLR model to monitor the dynamics of burned areas in the Mongolian grasslands, demonstrating that the dead fuel index was the most effective variable. Lu et al. [6] investigated the sensitivity of different fire indices derived from Landsat images to burned areas and degrees, which demonstrated that the mid-infrared burn index (MIRBI) had the most potential of these indices. The results also pointed out the superior performance of mid-infrared bands in monitoring post-fire residues. Finally, Li et al. [171] directly adopted MODIS NDVI or NPP productS as the substitute for fuel and utilized its time series for fire detection and dynamic analysis.

It is worth noting that a burned area product, MCD64A1, has been freely available from MODIS since 2001 [172], after which time many studies have employed it on various types of ecosystems. Alvarado et al. [173] directly adopted MCD64A1 data and investigated the effects of antecedent rainfall and fuel moisture on fire through MLR models, which demonstrated that fires in different grasslands might show contrasting responses to these two variables. However, the low temporal resolution of MODIS images restricted the accuracy of the MCD64A1 product. In 2020, Scholtz et al. [46] compared the differences between the MCD64A1 product and its customized products in Kansas Flint Hills Tall Grass Prairie. Their results showed a significant underestimation of the burned area by the MCD64A1 product. Therefore, the combination with ground measurements was suggested in the use of the MCD64A1 product. Meanwhile, Cai and Wang [174] adopted Landsat images and calculated the difference normalized burn ratio (dNBR) and the relative dNBR, both of which were associated with burn severity by a linear regression model and achieved comparable performance in grasslands.

In addition to the above studies that directly focused on the dynamic, some others worked on the relationship between environmental factors and fire. Li et al. [12] investigated the influence of land use on fire events. The results indicated a significant linear relationship between land use intensity and the number of fire events. Similarly, Dara et al. [175] mapped the burned area of grasslands in northern Kazakhstan between 1989 and 2016, which demonstrated the significant increase in burn area was strongly related to agricultural land use. Apart from land use, climate factors were also investigated [176,177]. In [176], a Gaussian generalized linear model was established to verify the correlation among climate factors and burned area, which showed that extreme rainfall events had the potential to predict burned areas in arid grassland. In [177], a multivariate nonlinear regression model was constructed between climate factors and the number of fire events, which indicated that climate factors such as temperature, precipitation, and humidity were obviously correlated with the number of fire events.

Third, for impact analysis, without human interference fire can cause irreversible effects on grassland ecosystems such as the reduction of biodiversity, the invasion of other species, and changes in soil structure. Therefore, the analysis of post-fire impacts is essential for making grassland restoration policies, leading to the recovery in the direction expected by human beings. For vegetation recovery, Lu et al. [6] investigated the recovery progress of semiarid grasslands after fire, which showed that the progress was highly affected by water availability and burn severity. Adagbasa et al. [178] developed a vegetation response ability model to simulate the vegetation recovery in a mountain grassland in which environmental factors, adaptation strategies, and ecological status were taken into account. In [178], a vegetation recovery index was created for model validation and was calculated based on the NDVI before and after the fire. The results demonstrated that both elevation and fire severity were highly important factors influencing the recovery. Steiner et al. [179] focused on the dynamic changes of the LSWI, the NDVI, and GPP after fire. In [179], GPP was estimated by a VPM model and had a distinct response to fire, which was first suppressed for a short time and then grew rapidly. Recently, Han et al. [180] investigated the short-term effects of fire severity on the recovery; LAI and FVC were estimated by a PROSAIL model to represent the vegetation status, which indicated that a certain extent of fire would stimulate the increase of the LAI and FVC.

Finally, for other impacts, Ratajczak et al. [181] found that the burned areas were susceptible to the invasion of shrubs and trees, which were difficult to reverse once the grassland was converted to shrubland and woodland. Ling et al. [13] investigated the impact on canopy nitrogen content. In their research, the canopy nitrogen content was retrieved based on a regression model using hyperspectral images from an airplane. Variogram analysis and heterogeneity metrics were applied to analyze the impacts, and the results showed an apparent and transient fire stimulus to plant growth, causing a short-term increase in canopy nitrogen content.

3.3.2. Drought

Drought is a cyclical climatic process but also a costly natural disaster. Prolonged drought may destroy widespread vegetation and accelerate the desertification of grasslands [43]. The research on grassland drought has been going on for a long time [182]. Typically, the occurrence of drought is frequently associated with longer periods of no rainfall as well as other factors such as temperature, evaporation, and human activities. On this basis, some remote sensing indices have been directly applied for its monitoring, such as the water condition index (WCI), the temperature condition index (TCI), the precipitation condition index (PCI), the soil moisture condition index (SMCI), the standardized precipitation index (SPI), the vegetation health index (VHI), and the vegetation condition index (VCI).

Muthumanickam et al. [183] applied the VCI for drought monitoring, which set thresholds to detect different drought stress levels. Cao et al. [184] applied the temperature vegetation dryness index calculated only by surface temperature to analyze the drought frequency in the Mongolian grasslands. However, more studies fused the above indices to improve the stability. Zhang et al. [185] proposed a new drought index, the microwave integrated drought index, for monitoring short-term drought in semiarid regions. PCI, TCI, and SMCI were retrieved from radar images to construct this index, which was proved to outperform other single microwave indices. Then, another index named the grassland drought index was built in [19] in which PCI, SMCI, and canopy water content were adopted in an MRL model. The validation of this index was successfully performed at regional scales as well as at larger scales. In 2021, Hermanns et al. [186] made full use of hyperspectral images. They combined a standardized precipitation evapotranspiration index (SPEI), a fused index considering potential evapotranspiration and precipitation, with ground-measured soil moisture to represent the drought stress. However, the evaluation of their results was performed using geophysical measurements and vegetation indices as proxy variables so that it needed further verification with ground data. In addition, Chang et al. [187] verified the performance of nine indices on Mongolian grasslands, which suggested that the combined use of a normalized difference water index and the VHI was most suitable for drought monitoring. Then, depending on their results, Chang et al. [43] further established a new drought index based on a PCA algorithm using the VHI, the WCI, and the TCI, which proved to be more suitable for drought monitoring in arid and semiarid grasslands. Meanwhile, Wei et al. [182] compared many single variable indices and fused indices, demonstrating that although these indices varied in performance under different conditions, fused indices were better overall than single indices for monitoring. They also pointed out that the empirical-based approach worked better than the constrained optimization approach for determining the weights of different variables in the construction of fused indices.

As for the impact analysis caused by drought, many surveys have focused on the changes of vegetation growth, which was highly related to vegetation indices and parameters. In 2012, Liu et al. [188] directly adopted the SPI to represent the degree of drought and the NDVI to represent the status of vegetation, which showed that the vegetation growth rate was most affected by drought, but the responses were varied among different types of grasslands. Then, Li et al. [189] also combined the NDVI representing vegetation condition with an effective drought index that was calculated only by precipitation data

to investigate the short-term response of grassland vegetation to drought. Apart from a single variable drought index, SPEI was adopted for drought degree in [190], where the NDVI was also used for vegetation status and its response. The results showed a significant positive relationship between the fused index and the degree of vegetation degradation.

In addition, some grassland parameters were also utilized for the impact analysis. Villarreal et al. [191] studied the combined effects of drought and fire, which adopted the Palmer drought severity index for drought degree and utilized the SAVI and the NDVI to estimate FVC. The dynamic changes indicated that the prescribed fire might stimulate the growth of vegetation during dry periods in desert grasslands. Ding et al. [192] applied vapor pressure deficit, a fused index combining air pressure, temperature, and specific humidity, to investigate the impact of atmospheric drought on GPP. The results demonstrated that atmospheric drought had a significant negative impact on GPP, and although this effect could be mitigated by the increase of carbon dioxide content, it could not be fully restored. Then, Chen et al. [193] investigated the impact on NPP and net ecosystem productivity in which the SPEI, the NDVI, and ground-measured AGB were utilized. In detail, NPP was obtained by the CASA model, and net ecosystem productivity was calculated by an infrared gas analyzer. Their results also showed a negative impact, but the impact could be rapidly compensated for under wetting conditions after drought, which indicated the robust capacity of ecosystems to recover and regenerate. In [194], the impact on biomass was studied. In detail, they first established a rule-based piecewise regression model to separated the influence of other factors from that of drought and verified the effectiveness of different drought indices. The results showed that the SPI, U.S. drought monitor index, and the evaporative stress index were more suitable in different vegetation growth periods of semiarid grasslands.

Finally, the moderating capacity of species diversity and functional diversity in dune grasslands to deal with drought was studied in [195] in which the SPEI and the NDVI were applied, and the diversity was represented by ground measurements. The results showed that rich species diversity could resist the negative effect of drought to some extent, while functional diversity had no significant effect. Then, the effects on grassland phenology were investigated in [196], where the SPEI was also adopted, which indicated that drought could lead to an earlier start and a later end to the growing season of grasslands. The impact on soil moisture was studied in [197]; the temperature vegetation dryness index was applied and showed a strong linear correlation with ground soil moisture data. Han et al. [198] explored the impacts on the evapotranspiration in semiarid grassland. In [198], the SPEI was used to represent drought degree and the results showed that the increase in the frequency and duration of drought did not certainly lead to significant changes in evapotranspiration; however, the increase in the drought degree was significantly associated with its decrease.

In conclusion, almost all studies directly employ remote sensing indices for drought monitoring, and most of these indices are strongly related with precipitation and the water content of vegetation or soil. Some parameters such as the AGB and GPP are estimated only as the responses in the impact analysis.

3.3.3. Other Disasters

Apart from fire and drought, grasslands are also exposed to other disasters such as snowstorms and earthquakes, but few studies have been conducted with grasslands as the sole site of study. In 2013, Wang et al. [199] established a multivariate nonlinear regression model for the warning of snow disasters in which snow cover and snow depth were obtained from optical and radar data, respectively. In 2019, Shao et al. [20] proposed a new index based on remote sensing and ground data to describe the resilience of the Tibetan Plateau grasslands to snow disasters. Yang et al. [200] monitored the vegetation recovery of different vegetation types including grasslands after an earthquake where the time series of MODIS NDVI were used to represent the vegetation status. For hurricanes, Hu et al. [201] surveyed the extent of destruction caused by hurricanes to different types of vegetation on the islands of Dominica and Puerto Rico in which the NDVI was also utilized

to indicate the damage severity. The results showed that grasslands were the least sensitive to hurricanes compared to forests, wetlands, and built-up areas.

3.4. Carbon Cycle Monitoring

Carbon cycle monitoring has always been one of the hot topics in ecosystem research. Grasslands store large amounts of carbon in both soil and vegetation, which occupies an essential position in the study of the carbon cycle. In this field, carbon flux is one of the most basic and critical concepts, expressing the total amount of carbon in an ecosystem passing through a certain ecological section. In grasslands, it is usually defined as the total amount of carbon cycled per unit area per unit time.

It is worth noting that the definition of carbon flux is similar to that of NPP and GPP. Thus, many studies directly utilized NPP or GPP to represent it. In 2014, Sakowska et al. [202] applied GPP for the monitoring of carbon flux in a subalpine grassland. GPP was estimated based on a linear regression model using the red-edge NDVI. Then, Umair et al. [203] also utilized GPP for carbon flux, and they further researched the effect of soil moisture, temperature, relative humidity, and solar radiation on the dynamics of carbon flux. In [203], the performance of GPP products from three different sources was compared, but the results showed that there was no robust product, and all had overestimation problems in some cases. Chen et al. [204] researched the carbon use efficiency of different terrestrial ecosystems, which can be defined as the ratio between NPP and GPP. In [204], NPP was estimated by subtracting the respiratory consumption component from MODIS GPP products. The component was calculated by MODIS LAI products, and the results showed that precipitation strongly affected carbon use efficiency in grasslands.

On the other hand, research has gradually developed into carbon uptake and carbon emission in which carbon dioxide is the main form of circulation. An ecosystem can be defined as a carbon sink or carbon source depending on whether it is a net absorber or a net emitter of carbon dioxide. The concept of net ecosystem exchange (NEE) and net ecosystem productivity (NEP) has been introduced to describe the property and capacity of grassland carbon sources and carbon sinks in many studies. In contrast to NPP, NEE or NEP further considers the effect of heterotrophic respiration, which mainly exists in the soil. Thus, they can generally be calculated by subtracting soil respiration from NPP or subtracting ecosystem respiration from GPP.

In 2015, Yan et al. [205] established a semi-empirical model to estimate the NEE in alpine grasslands. In detail, only ground-measured data were first applied for the construction of the model. Then, GPP was estimated by a rectangular hyperbola function of photosynthetically active radiation while ecosystem respiration was estimated by an exponential function of soil temperature. The parameters in both functions were retrieved from correlated remote sensing vegetation indices. However, the results showed that the performance of the model was limited by soil water content. Subsequently, some LUE models were utilized for the estimation. Berberoglu et al. [206] applied the CASA model to estimate NEP and studied the impact of climate on the carbon cycle in the Mediterranean watershed. Balzarolo et al. [14] focused on the relationship between carbon flux and some hyperspectral vegetation indices. The genetic algorithm and RF model were combined for the selection of optimal indices, and a LUE model was used for the estimation of NEE. However, their results indicated that there was no universal vegetation index suitable for all types of grasslands. Then, Dai et al. [207] also adopted the spatiotemporal characteristics of NEP to study the dynamics of carbon sources and sinks in the Inner Mongolia grasslands. In [207], NPP was estimated based on a LUE model, while soil respiration from ground-measured data was used to calculate NEP, and the impact of climate factors was analyzed, which showed that the effect of precipitation was significant. Nestola et al. [208] utilized NEP to investigate seasonal carbon dynamics, which also established a light-use efficiency model to track seasonal carbon flux.

Furthermore, Noumonvi et al. [209] adopted both GPP and NEE to represent carbon flux. Three linear regression models based on different constraints (none, photosynthetically

active radiation, LUE) were compared. The results demonstrated that the unconstrained model performed better overall, and the NDVI, the LSWI, and a modified normalized difference water index were, respectively, suitable for the estimation in different growth stages. In addition, the regional carbon flux maps were obtained in [209] for research on the spatial variation of the carbon cycle. In [210], NEE was calculated by GPP and ecosystem respiration, and the relationship between precipitation and carbon flux was also investigated in which GPP products from MODIS were utilized to represent the carbon flux. The carbon balance was also investigated in [210] through the effect of precipitation legacy on NEE. The results showed that precipitation legacy determined the carbon balance of semiarid grasslands by its significant effect on NEE.

In addition, carbon stock is also an important index in the carbon cycle. In 2013, Kazar et al. [211] directly adopted the AGB, which was estimated by an MLR model using a Landsat EVI and vegetation greenness products, to monitor the carbon storage on reclaimed grasslands. Then, Xia et al. [212] constructed a nonlinear regression model based on the NDVI to estimate NPP as the proxy for mapping and monitoring the dynamics of biomass carbon stock on a global scale. Ma et al. [7] combined the EVI and ground-measured data using spatially stratified sampling to estimate different components of carbon stock in typical, meadow, desert, and alpine grasslands. Ding et al. [213] applied a regression-kriging model and a hybrid geostatistical method, for the estimation in typical grassland and meadow grassland. The results showed that the model based on the NDVI achieved the best performance for a typical grassland, while the model based on the chlorophyll index worked best for meadow grassland. In addition, in [7], the total carbon stock were divided into the AGB, below-ground biomass, and soil organic carbon, and the results showed that soil organic carbon dominated the carbon storage in all cases. Therefore, for the estimation of soil organic carbon, Dai et al. [214] directly constructed a linear regression model based on the NDVI. Li et al. [215] built a TECO-R model based on the NDVI, which is an improved version of the CASA model and proved its robust performance in their experiments. In 2021, Venter et al. [216] took numerous ground data, satellite indices, and products as input to an RF model and mapped the soil organic carbon stocks in South Africa.

In conclusion, the monitoring of the carbon cycle is highly associated with productivity parameters (NPP, GPP, NEP). Most of their estimation model is based on LUE with few regression models being used. In addition, carbon cycle monitoring has lacked a comprehensive monitoring framework and evaluation system.

4. Discussion

4.1. Statistical Analysis for Remote Sensing Data

Based on the 196 publications collected in this paper, we first counted the number of publications using remote sensing data from different platforms, respectively. There is no doubt that the vast majority of studies work with satellite data. Therefore, we further counted the number of times different satellites appearing in these studies, and the top six frequent satellites are shown in Figure 1. It is worth noting that some studies [61,87,154,160] combined the use of images from different satellites so that these studies were counted multiple times according to the number of satellites involved.

Obviously, the number of appearances of Terra and Aqua satellites is overwhelmingly superior to others. The data from Terra and Aqua used in most studies is mainly provided by a MODIS sensor, which is a multispectral sensor providing 36 spectral bands from visible to thermal infrared range. Since Terra and Aqua satellites are in sun-synchronous orbits, the temporal resolution of MODIS images is 1 day. In addition, the MODIS sensor can also provide multiple vegetation indices and products. Especially for the NDVI, the vast majority of studies have directly used the NDVI product named MOD13Q1 from the MODIS sensor, which is also the main reason why Terra and Aqua satellites appear most frequently in this field. MOD13Q1 products have a temporal resolution of 16 days and a spatial resolution of 250 m, 500 m or 1 km. In addition, other NDVI datasets are contributed by the Global Inventory Modelling and Mapping Studies using NOAA satellite data and

by the VEGETATION PROCESSING Centre using SPOT satellite data, and these NDVI datasets were also adopted in some studies [125,164]. The NOAA NDVI dataset has a spatial resolution of 8 km and a temporal resolution of 15 days, while the SPOT NDVI dataset is constructed with a spatial resolution of 1 km and a temporal resolution of 10 days.

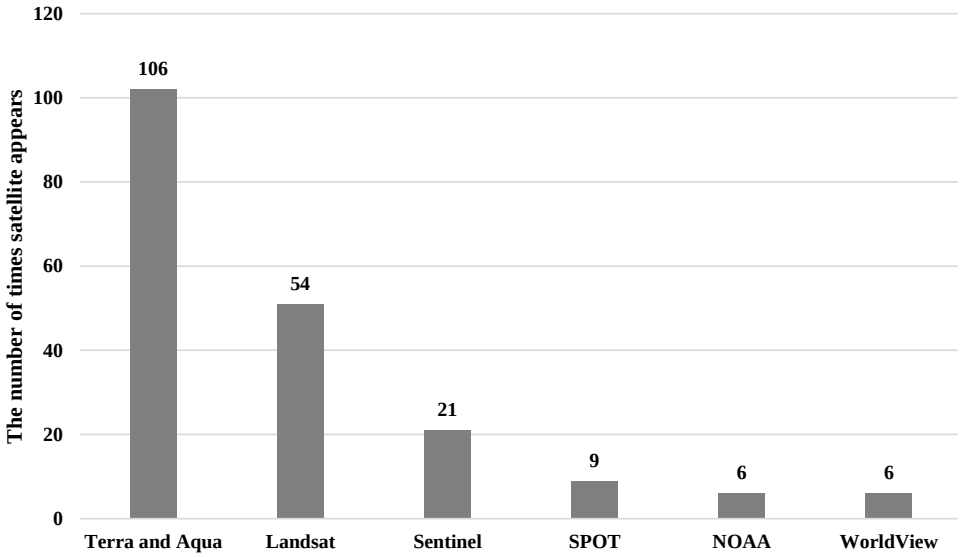

Figure 1. The number of times the top six frequently occurring satellites in 196 publications.

However, the temporal and spatial resolution of these products and datasets is relatively poor, which is not adequate for some studies [64,153,157]. Thus, many studies preferred to manually calculate the NDVI and some other remote sensing indices using raw spectral bands with high resolution from other satellites such as Landsat and Sentinel satellites [11,145,174,211]. For Landsat satellites, the thematic mapper, enhanced thematic mapper plus, and operational land imager are their main sensors, which also belong to the multispectral sensors. Compared to MODIS images, Landsat images have better spatial resolution (15 m, 30 m, 60 m) but have fewer spectral bands and a longer repeated observation period (16 days). Meanwhile, the multispectral instrument sensor is the main multispectral sensor carried by Sentinel satellites, generating optical images of 13 spectral bands with high spatial resolution (10 m, 20 m, 60 m) and a temporal resolution of 5 days. Despite the good spatial resolution of these images, they are separated in time by relatively long intervals, and their information is often obscured by cloud cover. As a result, several studies [68,154] fused these images from different satellites to complement missing information and to enhance the temporal continuity. In addition, many studies [22,24,63,103] installed multispectral sensors or RGB cameras on UAVs to acquire near-surface multispectral images. Compare with satellite images, these images have a much finer spatial resolution, usually less than 10 m, and they are not affected by cloud cover. However, these images only cover a small region and require a large number of repeat flights to ensure the time continuity, which does not fundamentally solve the problems.

Apart from multispectral images, some hyperspectral images are provided by EO-1 and HJ-1A satellites. These images have been utilized for AGB estimation [38] and the monitoring of degradation [8] and grazing [148]. However, compared to multispectral images, they are rarely used in research due to their massive redundant information. Even in the above relevant studies [8,38,148], the researchers only selected relevant bands based on the characteristics of the grasslands they were studying to calculate or create some vegetation indices whose performance is compared to determine the most appropriate index for the research. In addition, this strategy has also been applied to ground-based hyperspectral images [26,123]. In addition, these ground-based hyperspectral images were utilized for the simulation of multispectral images from satellites in [28,67] and for the

replacement of ground measurements in [104,108]. However, none of the above studies makes full use of the rich spectral information of hyperspectral images.

Finally, some studies [18,69,117] have made use of radar data, especially the SAR images. These SAR images can usually be acquired from ALOS, Sentinel, and Aqua satellite. Compared to optical images, the greatest advantage of SAR imagery is its ability to penetrate cloud cover to obtain information. Some research used them alone and proved their potential for estimation [69] and monitoring [16,17]. However, the utilization of SAR images is also limited by the low spatial resolution and some environmental interference. Fortunately, many studies [18,61,117] fully demonstrated the effectiveness of their combined use with optical images in enhancing model performance.

4.2. Characteristic Analysis of Estimation Methods and Monitoring Applications

Estimation Methods

From Tables 2–5, we can see that statistical regression and machine learning are the two main types of estimation methods. Especially in the estimation of the AGB, all the studies were based on these two methods. For statistical regression, all the models started by selecting some remote sensing-based vegetation indices related to the estimated parameter based on prior knowledge and performed correlation analysis between them, after which the most relevant one or several vegetation indices were extracted to construct the models based on a pre-assumed functional relationship. As for machine learning, we can see that RF and ANN models are more commonly used than others. In particular, many recent studies based on machine learning have started to combine ground-measured data and remote sensing data as the driving variables of their models and have shown that it can lead to better performance [47,73]. In addition, many studies have demonstrated that machine learning models outperform statistical regression models. However, based on the results in these tables, we can find that some of the machine-learning-based results are not excellent and sometimes even worse than the results of statistical regression models.

Apart from statistical regression and machine learning, some traditional methods that estimate parameters at the field scale using ground data only boost their estimation scales by combining remote sensing data and have been developed by many studies for the estimation of primary production, FVC, and LAI. For primary production, the light utilization efficiency approaches have proven to be effective in most cases, especially the CASA model that has been widely used in many studies. As shown in Table 3, some of the light utilization efficiency approaches can obtain comparable or even superior results to statistical regression methods. Then, for FVC, there have also been some studies focusing on mixed pixel decomposition methods in which the linear pixel dichotomy model based on the NDVI was most frequently used, while for the LAI, the radiative transfer models have been commonly used, especially the PROSAIL model. From Tables 4 and 5, we can also see the excellent performance of these traditional methods in some cases when compared to statistical regression and machine learning models.

In terms of the selection of driving variables for the above models, we can see that some studies [18,26,38,39] directly chose some well-established and robust indices, such as the NDVI, the EVI, the SAVI, and the CAI. Due to the strong absorption of red and blue light and the strong reflection of near infrared light by vegetation, the NDVI and the EVI were frequently used to reflect the state of vegetation and the spatial density distribution of vegetation. In some cases, some models driven only by the NDVI could achieve remarkably precise results [35,80,98] with R^2 over 0.9. However, in alpine and arid grasslands, as well as some grasslands with high spatial heterogeneity and complex grass species, the NDVI and the EVI generally did not obtain acceptable results. The models driven by the NDVI or EVI in [68,77] failed to obtain robust results with R^2 less than 0.5. Therefore, in response to this problem, many more suitable vegetation indices were developed or created based on the respective characteristics of the vegetation and environment under different studies [26,38]. Some of these studies also further considered and quantified the interference of environmental factors (phenology, precipitation, temperature) [76,89,94] and human

activities (population, land use, grazing) [34,48,73]. In addition, many studies have started to feed large amounts of raw data or spectral bands directly into MLR models or machine learning models [28,105,106]. According to their results presented in tables, most of the above refinements have achieved some certain effect.

4.3. Monitoring Applications

From an overall perspective, although part of the studies used the estimation methods covered in this paper to retrieve some parameters, the majority of studies directly used remote sensing data or satellite products. For grassland degradation monitoring, previous research directly made use of spectral bands and vegetation indices such as the SAVI, the MSAVI, and the RVI. After that, some estimated parameters are utilized. It can be seen that NPP and FVC have been frequently used in many studies, and almost all of these studies have applied the CASA model for the estimation of NPP and the mixed pixel decomposition model for FVC. Finally, some recent studies have begun to take some soil indices into account, but most of these indices were measured from ground observation [10,132,135].

In the monitoring of grassland use, many studies of grazing monitoring have also adopted some vegetation indices and estimated parameters, which is similar to the development of research on degradation monitoring. The difference is that the AGB has been most frequently used and in some cases has been combined with total biomass and FVC [30,141]. Moreover, the estimation models of the AGB in these studies have not been in a uniform form. Most of them are statistical regression models based on the NDVI or other vegetation indices. In addition, due to the limitations of the NDVI, recent studies have tended to apply or design some more robust vegetation indices such as NCI [30], CV [146], GII [143], and REP [149]. In contrast, for mowing monitoring, due to the temporal sensitivity of the mowing events, all the studies share the same strategy. In detail, the growth state of the vegetation has been simulated by the NDVI time series in most studies, and some potential mowing events have been discovered when comparing the simulated state with the ideal state and have been further analyzed to verify their authenticity. The latest research has focused on generating finer time series to improve the accuracy of monitoring [11,154,155].

For disaster monitoring, some specialized estimated parameters (curing degree, fuel biomass, LFMC) and remote sensing indices (PCI, TCI, SMCI) have been adopted in most studies. Some indices and products of fire from remote sensing satellites have been utilized in fire monitoring such as MIRBI [6] and MCD64A1 [46]. Similarly, some drought indices driven by single variable and multiple variables have been applied in drought monitoring, and the multivariate or fused indices have proved to have better performance in many studies [182,187]. Meanwhile, some estimated parameters have been employed in the impact analysis of disasters. It can be seen that the canopy nitrogen content, FVC, and the LAI have been utilized in the fire impact analysis [13,179,180], while the AGB and GPP have been involved in the drought impact analysis [192–194,196].

Finally, for carbon cycle monitoring, NPP and GPP have been fully utilized, and some new parameters such as NEP and NEE have been created based on them. The estimation of these indices in previous studies was mainly based on regression models. In contrast, recent studies have mainly focused on LUE approaches.

4.4. Limitations

Based on the above work, we have summarized the following limitations of remote sensing image processing technology in grassland studies.

Due to technical limitations, obtaining higher spatial resolution images means longer intervals between repeated shots, which also implies the reduction in temporal resolution. Reflecting on parameter estimation and applications, we can gain more accurate information and results by adopting higher spatial resolution images, but lower temporal resolution can lead to serious losses. On the one hand, high quality spatial information is necessary. It can be seen that MODIS images were most frequently adopted in most previ-

ous studies, but their poor spatial resolution had always impeded further improvements of the results. In particular, some MODIS products even suffer from severe underestimation of ground-measured values in some cases [34,45,46]. Therefore, since the launch of many advanced satellites, most subsequent studies have begun to rely on remote sensing images with better spatial quality such as Landsat and Sentinel images, which have achieved certain enhancements and breakthroughs in the results. On the other hand, the decrease in temporal resolution inevitably leads to a number of problems. Especially in the monitoring of mowing events, which are more sensitive to temporal resolution, the key of the research is the accurate construction of time series of some related indices or estimated parameters, where high temporal resolution is very critical to the results despite the fact that the quality of spatial information also plays a role.

In addition, all these common remote sensing images belong to optical images, which will inevitably be affected by cloud cover and shadowing, resulting in the lack of spatial information and breaks in temporal continuity. Although there were a few studies utilizing UAV or airplane images [23,186] and radar data [19,117,185], it still has failed to fundamentally solve the problem. UAV images have significant limitations on the shooting locations and coverage size. For radar images, the emitted microwaves can pass through the clouds and fogs and do not require lighting conditions, which means that they can work all the time. Meanwhile, they are also sensitive to water-related information, such as material water content, soil moisture, and humidity, which are suitable for drought monitoring. However, radar images can also be disturbed by other environmental factors and the spatial resolution of radar images is much lower than that of optical images, which restricts the wide applications of radar images.

Tuning to the perspective of estimation methods, most parameters were estimated based on statistical regression models in the applications. More notably, among these models, univariate models were the most common. However, statistical regression models are not good at elucidating the complex mechanisms of change in parameters, especially those univariate models that are more susceptible to interference. As shown in Tables 2–5, we can find that some univariate models can give the best results. However, it is mainly attributed to the simple spectral characteristics of the grassland they study, and it can also be seen that more univariate models give very poor results in alpine and arid grasslands. Therefore, the relationship established by univariate statistical regression models for a certain type of grassland cannot be transferred to other regions or larger scales that contain various types of grasslands or with high spatial heterogeneity.

Another main class of approaches is machine learning, such as RF, ANN, and SVM, which have stronger generalization ability and can be easily fit to nonlinear relationships. Although this type of method allows more variables as input to improve the stability and the resistance against disturbances, excessive input variables not only lead to a loss of efficiency but also do not always yield the best results. Many studies have tried different combinations of variables, most of which determined the variables based on significance and correlation analysis. The optimal combination of variables for different types of grasslands and study sites can vary greatly, but there has been a lack of uniform and comprehensive criteria. In addition, the training of machine learning models requires large amounts of remote sensing data. Although non-parametric models can generally get better results, their accuracy significantly depends on the quantity and quality of statistical data. In practice, it is complex and time-consuming to obtain a large amount of field statistical data to match remote sensing data for the same study area, and the registration problems between various data sources can also dramatically affect the results. As a result, the non-parametric model may not perform better than the parametric model under the condition of less available data, as shown in Tables 2–5.

In addition, some specific models and integrated frameworks based on certain theories or previous research are fully utilized, but they also face the problem of generalization. For example, the CASA model is preferred for the estimation of NPP in most studies for all kinds of grasslands, but it was originally established based on the vegetation conditions in

North America. Therefore, the model structure and some empirical parameters need to be adjusted according to the characteristics of the study area. Simultaneously, there may also be challenges in obtaining some necessary indices, especially the required soil indices. The accuracy of these indices can severely affect the results.

Although a number of innovative estimation methods have been proposed, they have not been adopted in the applications. The estimation methods applied in most applications are still stuck on simple linear models, which require further breakthroughs.

Finally, when it comes to the use of remote sensing data, the NDVI has always been the first and preferred index to be considered in all fields, but it is hard to cope with grasslands under extreme weather or complex environments. Other popular indices such as the EVI, the RVI, and the SAVI also face the same problem. The causes can be attributed mainly to both environmental and human factors. On the one hand, according to [217,218], greenness-based vegetation indices are highly correlated with soil moisture, and this correlation can also be influenced by soil properties, topography, and climate. Therefore, in arid and semiarid regions, where vegetation is dry or senescent for most of the year, the robustness of these green-based vegetation indices in monitoring vegetation status is significantly diminished. It can be seen that [219,220] demonstrated that the variability of some green-based vegetation indices during the dry season was mainly influenced by solar illumination effects rather than the changes in vegetation. In addition, the NDVI has also proved to be very sensitive to soil optical properties under conditions of incomplete vegetation cover [26,38], which can result in the effectiveness of the NDVI being susceptible to the soil background noise when vegetation is sparse. In contrast, when vegetation is dense, especially when the density reaches a certain threshold, the NDVI will become saturated and insensitive to vegetation growth. On the other hand, many human factors can also affect the accuracy of grassland monitoring, especially some human activities such as grazing and mowing which can result in some abrupt changes in vegetation status. How to accurately quantify and promptly track these human activities has always been an issue in this field. However, few studies have directly considered feeding these human factors into their models, and many of them have just conducted some impact analysis during model validation.

4.5. Future Work

The application of remote sensing technology in grassland study has been booming and has achieved certain achievements. However, through the above analyses, we can also put forward several suggestions for future work.

First, the combination of optical and radar images should be considered. Although radar images have started to be applied in many fields, their utilization has been limited by the low spatial resolution and some environmental interference. Meanwhile, the optical images are always suffering from interference from clouds and fogs. Thus, we should make full use of the complementary information of both to eliminate the defects. Furthermore, we can see that Griffiths et al. [154] synthesized Sentinel-2 and Landsat-8 optical images to improve the temporal resolution of images with the maintenance of spatial resolution and achieved better results. Similarly, some studies [85,86] fused Landsat and MODIS data to the constructed NDVI with high spatial and temporal resolution, achieving significant improvements in estimation accuracy. Following these ideas, we can also apply image fusion technology to address the irreconcilable conflict between spatial and temporal resolution. Meanwhile, this technology can also be used to improve the availability of hyperspectral images.

Second, most researchers working on the monitoring applications should consider further exploiting the potential of parameter estimation methods rather than directly using non-robust satellite products, especially when studying some unusual grasslands with extremely complex conditions. Meanwhile, those researchers who have already used the estimated parameters should adopt advanced estimation methods instead of simply working with linear regression models or other univariate models. In particular,

although the NDVI has many limitations as we mentioned above, it does not mean that the utilization of the NDVI should be abandoned. Some studies [63,93] have proved that the combined use of the NDVI can sometimes yield significant enhancements to their results. Thus, to obtain robust results, it is essential to select a right combination of variables according to the environmental and spectral characteristics of the grassland under study or to create more suitable vegetation indices [44].

Finally, we need to further adopt some new methods to improve the accuracy of the estimation. Since deep learning has proven its superior performance in processing high-dimensional data and nonlinear relationships, it has been widely used in many domains of image processing. However, very few studies have been conducted using this method in this area, and all of them have stayed on some shallow neural networks. We should further promote and explore the use of deep learning in this field. Especially, The high-dimensional data of hyperspectral images have been difficult to process by traditional methods, which also means that deep learning is a good choice to make full use of them. In addition, deep neural networks can also easily cope with multi-source inputs and can adaptively learn weights to fuse key information from them.

5. Conclusions

In this article, the remote sensing estimation methods of four key parameters of grasslands and their applications in remote sensing monitoring are reviewed. Based on the statistics and analysis of related work, we point out the limitations of current studies and make suggestions for future work. In general, although some machine learning methods and improved traditional methods have been proposed, most studies are still using simple statistical regression to estimate these parameters. Meanwhile, these methods have suffered from defects in the selection of driving variables and the generalization ability to different types of grassland. In addition, the quality of remote sensing images has also hindered the advancement of research. For these reasons, we recommend the combined use of different remote sensing images such as radar and optical images to take advantage of complementary information, which also means that image fusion techniques should be employed to generate high-quality images. Finally, deep learning is suggested to be applied in most domains due to its ability to process high-dimensional data and fit non-linear relationships, which can extract and make full use of valuable information from hyperspectral images or multi-source images, improving the accuracy and robustness of estimation results.

Author Contributions: Conceptualization, Z.W.; writing—original draft preparation, Y.M.; writing—review and editing, Z.W. and J.S.; project administration, Y.Z.; funding acquisition, Z.W. All authors have read and agreed to the published version of the manuscript.

Funding: This research was supported by National Natural Science Foundation of China (Grant No. 61201421), National cryosphere desert data center (Grant No. E01Z7902) and Capability improvement project for cryosphere desert data center of the Chinese Academy of Sciences (Grant No. Y9298302).

Data Availability Statement: Not applicable.

Conflicts of Interest: The authors declare no conflict of interest.

References

1. Arasumani, M.; Bunyan, M.; Robin, V.V. Opportunities and challenges in using remote sensing for invasive tree species management, and in the identification of restoration sites in tropical montane grasslands. *J. Environ. Manag.* **2021**, *280*, 111759. [CrossRef] [PubMed]
2. Reinermann, S.; Asam, S.; Kuenzer, C. Remote Sensing of Grassland Production and Management—A Review. *Remote Sens.* **2020**, *12*, 1949. [CrossRef]
3. Lu, D.; Batistella, M.; Mausel, P.; Moran, E. Mapping and monitoring land degradation risks in the Western Brazilian Amazon using multitemporal Landsat TM/ETM+ images. *Land Degrad. Dev.* **2007**, *18*, 41–54. [CrossRef]

4. Junges, A.H.; Bremm, C.; Fontana, D.C.; de Oliveira, C.A.O.; Schaparini, L.P.; Carvalho, P.C.d.F. Temporal profiles of vegetation indices for characterizing grazing intensity on natural grasslands in Pampa biome. *Sci. Agric.* **2016**, *73*, 332–337. [CrossRef]
5. Zhang, Z.; Feng, Z.; Zhang, H.; Zhao, J.; Yu, S.; Du, W. Spatial distribution of grassland fires at the regional scale based on the MODIS active fire products. *Int. J. Wildland Fire* **2017**, *26*, 209–218. [CrossRef]
6. Lu, B.; He, Y.; Tong, A. Evaluation of spectral indices for estimating burn severity in semiarid grasslands. *Int. J. Wildland Fire* **2016**, *25*, 147–157. [CrossRef]
7. Ma, Q.; Kuang, W.; Liu, Z.; Hu, F.; Qian, J.; Liu, B.; Zhu, J.; Cao, C.; Wu, J.; Li, X.; et al. Spatial pattern of different component carbon in varied grasslands of northern China. *Geoderma* **2017**, *303*, 27–36. [CrossRef]
8. Lyu, X.; Li, X.B.; Dang, D.L.; Dou, H.S.; Xuan, X.J.; Liu, S.Y.; Li, M.Y.; Gong, J.R. A new method for grassland degradation monitoring by vegetation species composition using hyperspectral remote sensing. *Ecol. Indic.* **2020**, *114*, 106310. [CrossRef]
9. Kong, B.; Yu, H.; Du, R.X.; Wang, Q. Quantitative Estimation of Biomass of Alpine Grasslands Using Hyperspectral Remote Sensing. *Rangel. Ecol. Manag.* **2019**, *72*, 336–346. [CrossRef]
10. Mansour, K.; Mutanga, O.; Adam, E.; Abdel-Rahman, E.M. Multispectral remote sensing for mapping grassland degradation using the key indicators of grass species and edaphic factors. *Geocarto Int.* **2016**, *31*, 477–491. [CrossRef]
11. Kolecka, N.; Ginzler, C.; Pazur, R.; Price, B.; Verburg, P. Regional Scale Mapping of Grassland Mowing Frequency with Sentinel-2 Time Series. *Remote Sens.* **2018**, *10*, 1221. [CrossRef]
12. Li, Y.; Zhao, J.; Guo, X.; Zhang, Z.; Tan, G.; Yang, J. The Influence of Land Use on the Grassland Fire Occurrence in the Northeastern Inner Mongolia Autonomous Region, China. *Sensors* **2017**, *17*, 437. [CrossRef] [PubMed]
13. Ling, B.; Raynor, E.J.; Goodin, D.G.; Joern, A. Effects of Fire and Large Herbivores on Canopy Nitrogen in a Tallgrass Prairie. *Remote Sens.* **2019**, *11*, 1364. [CrossRef]
14. Balzarolo, M.; Vescovo, L.; Hammerle, A.; Gianelle, D.; Papale, D.; Tomelleri, E.; Wohlfahrt, G. On the relationship between ecosystem-scale hyperspectral reflectance and CO_2 exchange in European mountain grasslands. *Biogeosciences* **2015**, *12*, 3089–3108. [CrossRef]
15. Braun, A.; Wagner, J.; Hochschild, V. Above-ground biomass estimates based on active and passive microwave sensor imagery in low-biomass savanna ecosystems. *J. Appl. Remote Sens.* **2018**, *12*, 46027. [CrossRef]
16. Ali, I.; Barrett, B.; Cawkwell, F.; Green, S.; Dwyer, E.; Neumann, M. Application of Repeat-Pass TerraSAR-X Staring Spotlight Interferometric Coherence to Monitor Pasture Biophysical Parameters: Limitations and Sensitivity Analysis. *IEEE J. Sel. Top. Appl. Earth Obs. Remote Sens.* **2017**, *10*, 3225–3231. [CrossRef]
17. Zalite, K.; Antropov, O.; Praks, J.; Voormansik, K.; Noorma, M. Monitoring of Agricultural Grasslands With Time Series of X-Band Repeat-Pass Interferometric SAR. *IEEE J. Sel. Top. Appl. Earth Obs. Remote Sens.* **2016**, *9*, 3687–3697. [CrossRef]
18. Wang, J.; Xiao, X.; Bajgain, R.; Starks, P.; Steiner, J.; Doughty, R.B.; Chang, Q. Estimating leaf area index and aboveground biomass of grazing pastures using Sentinel-1, Sentinel-2 and Landsat images. *ISPRS J. Photogramm. Remote Sens.* **2019**, *154*, 189–201. [CrossRef]
19. He, B.; Liao, Z.; Quan, X.; Li, X.; Hu, J. A Global Grassland Drought Index (GDI) Product: Algorithm and Validation. *Remote Sens.* **2015**, *7*, 12704–12736. [CrossRef]
20. Shao, Q.; Liu, G.; Li, X.; Huang, H.; Fan, J.; Wang, L.; Liu, J.; Guo, X. Assessing the Snow Disaster and Disaster Resistance Capability for Spring 2019 in China's Three-River Headwaters Region. *Sustainability* **2019**, *11*, 6423. [CrossRef]
21. Zhang, H.; Sun, Y.; Chang, L.; Qin, Y.; Chen, J.; Qin, Y.; Du, J.; Yi, S.; Wang, Y. Estimation of Grassland Canopy Height and Aboveground Biomass at the Quadrat Scale Using Unmanned Aerial Vehicle. *Remote Sens.* **2018**, *10*, 851. [CrossRef]
22. Shi, Y.; Gao, J.; Li, X.; Li, J.; dela Torre, D.M.G.; Brierley, G.J. Improved Estimation of Aboveground Biomass of Disturbed Grassland through Including Bare Ground and Grazing Intensity. *Remote Sens.* **2021**, *13*, 2105. [CrossRef]
23. Pi, W.; Du, J.; Liu, H.; Zhu, X. Desertification Glassland Classification and Three-Dimensional Convolution Neural Network Model for Identifying Desert Grassland Landforms with Unmanned Aerial Vehicle Hyperspectral Remote Sensing Images. *J. Appl. Spectrosc.* **2020**, *87*, 309–318. [CrossRef]
24. Chen, J.J.; Zhao, X.N.; Zhang, H.Z.; Qin, Y.; Yi, S.H. Evaluation of the Accuracy of the Field Quadrat Survey of Alpine Grassland Fractional Vegetation Cover Based on the Satellite Remote Sensing Pixel Scale. *ISPRS Int. J. Geo-Inf.* **2019**, *8*, 497. [CrossRef]
25. van der Merwe, D.; Baldwin, C.E.; Boyer, W. An efficient method for estimating dormant season grass biomass in tallgrass prairie from ultra-high spatial resolution aerial imaging produced with small unmanned aircraft systems. *Int. J. Wildland Fire* **2020**, *29*, 696–701. [CrossRef]
26. Ren, H.; Zhou, G.; Zhang, F. Using negative soil adjustment factor in soil-adjusted vegetation index (SAVI) for aboveground living biomass estimation in arid grasslands. *Remote Sens. Environ.* **2018**, *209*, 439–445. [CrossRef]
27. Rueda-Ayala, V.P.; Pena, J.M.; Hoglind, M.; Bengochea-Guevara, J.M.; Andujar, D. Comparing UAV-Based Technologies and RGB-D Reconstruction Methods for Plant Height and Biomass Monitoring on Grass Ley. *Sensors* **2019**, *19*, 535. [CrossRef]
28. Cerasoli, S.; Campagnolo, M.; Faria, J.; Nogueira, C.; Caldeira, M.d.C. On estimating the gross primary productivity of Mediterranean grasslands under different fertilization regimes using vegetation indices and hyperspectral reflectance. *Biogeosciences* **2018**, *15*, 5455–5471. [CrossRef]
29. Lu, B.; Dao, P.; Liu, J.; He, Y.; Shang, J. Recent Advances of Hyperspectral Imaging Technology and Applications in Agriculture. *Remote Sens.* **2020**, *12*, 2659. [CrossRef]

30. Yang, X.; Guo, X.; Fitzsimmons, M. Assessing light to moderate grazing effects on grassland production using satellite imagery. *Int. J. Remote Sens.* **2012**, *33*, 5087–5104. [CrossRef]
31. Wijesingha, J.; Moeckel, T.; Hensgen, F.; Wachendorf, M. Evaluation of 3D point cloud-based models for the prediction of grassland biomass. *Int. J. Appl. Earth Obs. Geoinf.* **2019**, *78*, 352–359. [CrossRef]
32. Xu, K.; Su, Y.; Liu, J.; Hu, T.; Jin, S.; Ma, Q.; Zhai, Q.; Wang, R.; Zhang, J.; Li, Y.; et al. Estimation of degraded grassland aboveground biomass using machine learning methods from terrestrial laser scanning data. *Ecol. Indic.* **2020**, *108*, 105747. [CrossRef]
33. Chu, D. Aboveground biomass estimates of grassland in the north tibet using modies remote sensing approaches. *Appl. Ecol. Environ. Res.* **2020**, *18*, 7655–7672. [CrossRef]
34. Ye, H.; Huang, X.-t.; Luo, G.-p.; Wang, J.-b.; Zhang, M.; Wang, X.-x. Improving remote sensing-based net primary production estimation in the grazed land with defoliation formulation model. *J. Mt. Sci.* **2019**, *16*, 323–336. [CrossRef]
35. Karimi, S.; Sadraddini, A.A.; Nazemi, A.H.; Xu, T.; Fard, A.F. Generalizability of gene expression programming and random forest methodologies in estimating cropland and grassland leaf area index. *Comput. Electron. Agric.* **2018**, *144*, 232–240. [CrossRef]
36. Zhang, W.B.; Yang, X.C.; Manlike, A.; Jin, Y.X.; Zheng, F.L.; Guo, J.; Shen, G.; Zhang, Y.J.; Bin, X. Comparative study of remote sensing estimation methods for grassland fractional vegetation coverage—A grassland case study performed in Ili prefecture, Xinjiang, China. *Int. J. Remote Sens.* **2019**, *40*, 2243–2258. [CrossRef]
37. Huete, A.; Didan, K.; Miura, T.; Rodriguez, E.; Gao, X.; Ferreira, L. Overview of the radiometric and biophysical performance of the MODIS vegetation indices. *Remote Sens. Environ.* **2002**, *83*, 195–213. [CrossRef]
38. Wang, G.; Liu, S.; Liu, T.; Fu, Z.; Yu, J.; Xue, B. Modelling above-ground biomass based on vegetation indexes: A modified approach for biomass estimation in semiarid grasslands. *Int. J. Remote Sens.* **2018**, *40*, 3835–3854. [CrossRef]
39. Li, M.; Wu, J.; Song, C.; He, Y.; Niu, B.; Fu, G.; Tarolli, P.; Tietjen, B.; Zhang, X. Temporal Variability of Precipitation and Biomass of Alpine Grasslands on the Northern Tibetan Plateau. *Remote Sens.* **2019**, *11*, 360. [CrossRef]
40. Lin, S.; Li, J.; Liu, Q.; Li, L.; Zhao, J.; Yu, W. Evaluating the Effectiveness of Using Vegetation Indices Based on Red-Edge Reflectance from Sentinel-2 to Estimate Gross Primary Productivity. *Remote Sens.* **2019**, *11*, 1303. [CrossRef]
41. Wu, Z.; Lei, S.; Bian, Z.; Huang, J.; Zhang, Y. Study of the desertification index based on the albedo-MSAVI feature space for semiarid steppe region. *Environ. Earth Sci.* **2019**, *78*, 232. [CrossRef]
42. Zhang, Y.; Zhang, C.B.; Wang, Z.Q.; An, R.; Li, J.L. Comprehensive Research on Remote Sensing Monitoring of Grassland Degradation: A Case Study in the Three-River Source Region, China. *Sustainability* **2019**, *11*, 1845. [CrossRef]
43. Chang, S.; Chen, H.; Wu, B.; Nasanbat, E.; Yan, N.; Davdai, B. A Practical Satellite-Derived Vegetation Drought Index for Arid and semiarid Grassland Drought Monitoring. *Remote Sens.* **2021**, *13*, 414. [CrossRef]
44. Xue, J.; Su, B. Significant Remote Sensing Vegetation Indices: A Review of Developments and Applications. *J. Sens.* **2017**, *2017*, 1353691. [CrossRef]
45. Zhu, X.; Pei, Y.; Zheng, Z.; Dong, J.; Zhang, Y.; Wang, J.; Chen, L.; Doughty, R.; Zhang, G.; Xiao, X. Underestimates of Grassland Gross Primary Production in MODIS Standard Products. *Remote Sens.* **2018**, *10*, 1771. [CrossRef]
46. Scholtz, R.; Prentice, J.; Tang, Y.; Twidwell, D. Improving on MODIS MCD64A1 Burned Area Estimates in Grassland Systems: A Case Study in Kansas Flint Hills Tall Grass Prairie. *Remote Sens.* **2020**, *12*, 2168. [CrossRef]
47. Meng, B.P.; Liang, T.G.; Yi, S.H.; Yin, J.P.; Cui, X.; Ge, J.; Hou, M.J.; Lv, Y.Y.; Sun, Y. Modeling Alpine Grassland Above Ground Biomass Based on Remote Sensing Data and Machine Learning Algorithm: A Case Study in East of the Tibetan Plateau, China. *IEEE J. Sel. Top. Appl. Earth Obs. Remote Sens.* **2020**, *13*, 2986–2995. [CrossRef]
48. Zheng, F.; Hu, Y.; Qibing, W.; Feng, Z. Changes and controls of aboveground net primary production in response to grassland policy in Inner Mongolian grasslands of China. *Remote Sens. Appl. Soc. Environ.* **2021**, *22*, 100526. [CrossRef]
49. Awuah, K.T.; Aplin, P.; Marston, C.G.; Powell, I.; Smit, I.P.J. Probabilistic Mapping and Spatial Pattern Analysis of Grazing Lawns in Southern African Savannahs Using WorldView-3 Imagery and Machine Learning Techniques. *Remote Sens.* **2020**, *12*, 3357. [CrossRef]
50. Zhou, W.; Yang, H.; Huang, L.; Chen, C.; Lin, X.S.; Hu, Z.J.; Li, J.L. Grassland degradation remote sensing monitoring and driving factors quantitative assessment in China from 1982 to 2010. *Ecol. Indic.* **2017**, *83*, 303–313. [CrossRef]
51. Transon, J.; D'Andrimont, R.; Maugnard, A.; Defourny, P. Survey of Hyperspectral Earth Observation Applications from Space in the Sentinel-2 Context. *Remote Sens.* **2018**, *10*, 157. [CrossRef]
52. Steele-Dunne, S.C.; McNairn, H.; Monsivais-Huertero, A.; Judge, J.; Liu, P.W.; Papathanassiou, K. Radar Remote Sensing of Agricultural Canopies: A Review. *IEEE J. Sel. Top. Appl. Earth Obs. Remote Sens.* **2017**, *10*, 2249–2273. [CrossRef]
53. Maes, W.H.; Steppe, K. Perspectives for Remote Sensing with Unmanned Aerial Vehicles in Precision Agriculture. *Trends Plant Sci.* **2019**, *24*, 152–164. [CrossRef] [PubMed]
54. Adão, T.; Hruška, J.; Pádua, L.; Bessa, J.; Peres, E.; Morais, R.; Sousa, J.J. Hyperspectral Imaging: A Review on UAV-Based Sensors, Data Processing and Applications for Agriculture and Forestry. *Remote Sens.* **2017**, *9*, 1110. [CrossRef]
55. Xiao, J.; Chevallier, F.; Gomez, C.; Guanter, L.; Hicke, J.A.; Huete, A.R.; Ichii, K.; Ni, W.; Pang, Y.; Rahman, A.F.; et al. Remote sensing of the terrestrial carbon cycle: A review of advances over 50 years. *Remote Sens. Environ.* **2019**, *233*, 111383. [CrossRef]
56. Xu, D.D.; Guo, X.L. Some Insights on Grassland Health Assessment Based on Remote Sensing. *Sensors* **2015**, *15*, 3070–3089. [CrossRef] [PubMed]

57. Wachendorf, M.; Fricke, T.; Moeckel, T. Remote sensing as a tool to assess botanical composition, structure, quantity and quality of temperate grasslands. *Grass Forage Sci.* **2018**, *73*, 1–14. [CrossRef]
58. Ali, I.; Cawkwell, F.; Dwyer, E.; Barrett, B.; Green, S. Satellite remote sensing of grasslands: From observation to management. *J. Plant Ecol.* **2016**, *9*, 649–671. [CrossRef]
59. Xu, D.; Chen, B.; Yan, R.; Yan, Y.; Sun, X.; Xu, L.; Xin, X. Quantitative monitoring of grazing intensity in the temperate meadow steppe based on remote sensing data. *Int. J. Remote Sens.* **2018**, *40*, 2227–2242. [CrossRef]
60. Grüner, E.; Astor, T.; Wachendorf, M. Biomass Prediction of Heterogeneous Temperate Grasslands Using an SfM Approach Based on UAV Imaging. *Agronomy* **2019**, *9*, 54. [CrossRef]
61. Naidoo, L.; van Deventer, H.; Ramoelo, A.; Mathieu, R.; Nondlazi, B.; Gangat, R. Estimating above ground biomass as an indicator of carbon storage in vegetated wetlands of the grassland biome of South Africa. *Int. J. Appl. Earth Obs. Geoinf.* **2019**, *78*, 118–129. [CrossRef]
62. Yang, S.X.; Feng, Q.S.; Liang, T.G.; Liu, B.K.; Zhang, W.J.; Xie, H.J. Modeling grassland above-ground biomass based on artificial neural network and remote sensing in the Three-River Headwaters Region. *Remote Sens. Environ.* **2018**, *204*, 448–455. [CrossRef]
63. Lussem, U.; Bolten, A.; Menne, J.; Gnyp, M.L.; Schellberg, J.; Bareth, G. Estimating biomass in temperate grassland with high resolution canopy surface models from UAV-based RGB images and vegetation indices. *J. Appl. Remote Sens.* **2019**, *13*, 34525. [CrossRef]
64. Clementini, C.; Pomente, A.; Latini, D.; Kanamaru, H.; Vuolo, M.R.; Heureux, A.; Fujisawa, M.; Schiavon, G.; Del Frate, F. Long-Term Grass Biomass Estimation of Pastures from Satellite Data. *Remote Sens.* **2020**, *12*, 2160. [CrossRef]
65. Zhang, X.; Chen, X.; Tian, M.; Fan, Y.; Ma, J.; Xing, D. An evaluation model for aboveground biomass based on hyperspectral data from field and TM8 in Khorchin grassland, China. *PLoS ONE* **2020**, *15*, e0223934. [CrossRef]
66. KarakoÇ, A.; Karabulut, M. Ratio-based vegetation indices for biomass estimation depending on grassland characteristics. *Turk. J. Bot.* **2019**, *43*, 619–633. [CrossRef]
67. Pang, H.; Zhang, A.; Kang, X.; He, N.; Dong, G. Estimation of the Grassland Aboveground Biomass of the Inner Mongolia Plateau Using the Simulated Spectra of Sentinel-2 Images. *Remote Sens.* **2020**, *12*, 4155. [CrossRef]
68. Zeng, N.; He, H.; Ren, X.; Zhang, L.; Zeng, Y.; Fan, J.; Li, Y.; Niu, Z.; Zhu, X.; Chang, Q. The utility of fusing multi-sensor data spatio-temporally in estimating grassland aboveground biomass in the three-river headwaters region of China. *Int. J. Remote Sens.* **2020**, *41*, 7068–7089. [CrossRef]
69. Bao, N.; Li, W.; Gu, X.; Liu, Y. Biomass Estimation for Semiarid Vegetation and Mine Rehabilitation Using Worldview-3 and Sentinel-1 SAR Imagery. *Remote Sens.* **2019**, *11*, 2855. [CrossRef]
70. John, R.; Chen, J.; Giannico, V.; Park, H.; Xiao, J.; Shirkey, G.; Ouyang, Z.; Shao, C.; Lafortezza, R.; Qi, J. Grassland canopy cover and aboveground biomass in Mongolia and Inner Mongolia: Spatiotemporal estimates and controlling factors. *Remote Sens. Environ.* **2018**, *213*, 34–48. [CrossRef]
71. Yin, G.; Li, A.; Wu, C.; Wang, J.; Xie, Q.; Zhang, Z.; Nan, X.; Jin, H.; Bian, J.; Lei, G. Seamless Upscaling of the Field-Measured Grassland Aboveground Biomass Based on Gaussian Process Regression and Gap-Filled Landsat 8 OLI Reflectance. *ISPRS Int. J. Geo-Inf.* **2018**, *7*, 242. [CrossRef]
72. Zeng, N.; Ren, X.; He, H.; Zhang, L.; Zhao, D.; Ge, R.; Li, P.; Niu, Z. Estimating grassland aboveground biomass on the Tibetan Plateau using a random forest algorithm. *Ecol. Indic.* **2019**, *102*, 479–487. [CrossRef]
73. Zhou, W.; Li, H.R.; Xie, L.J.; Nie, X.M.; Wang, Z.; Du, Z.P.; Yue, T.X. Remote sensing inversion of grassland aboveground biomass based on high accuracy surface modeling. *Ecol. Indic.* **2021**, *121*, 107215. [CrossRef]
74. Lyu, X.; Li, X.; Gong, J.; Li, S.; Dou, H.; Dang, D.; Xuan, X.; Wang, H. Remote-sensing inversion method for aboveground biomass of typical steppe in Inner Mongolia, China. *Ecol. Indic.* **2021**, *120*, 106883. [CrossRef]
75. Zhao, F.; Xu, B.; Yang, X.; Xia, L.; Jin, Y.; Li, J.; Zhang, W.; Guo, J.; Shen, G. Modelling and analysis of net primary productivity and its response mechanism to climate factors in temperate grassland, northern China. *Int. J. Remote Sens.* **2018**, *40*, 2259–2277. [CrossRef]
76. Zheng, Z.; Zhu, W.; Zhang, Y. Direct and Lagged Effects of Spring Phenology on Net Primary Productivity in the Alpine Grasslands on the Tibetan Plateau. *Remote Sens.* **2020**, *12*, 1223. [CrossRef]
77. Luo, Z.; Wu, W.; Yu, X.; Song, Q.; Yang, J.; Wu, J.; Zhang, H. Variation of Net Primary Production and Its Correlation with Climate Change and Anthropogenic Activities over the Tibetan Plateau. *Remote Sens.* **2018**, *10*, 1352. [CrossRef]
78. Jin, H.; Bao, G.; Chen, J.; Chopping, M.; Jin, E.; Mandakh, U.; Jiang, K.; Huang, X.; Bao, Y.; Vandansambuu, B. Modifying the maximal light-use efficiency for enhancing predictions of vegetation net primary productivity on the Mongolian Plateau. *Int. J. Remote Sens.* **2020**, *41*, 3740–3760. [CrossRef]
79. Nanzad, L.; Zhang, J.; Batdelger, G.; Pangali Sharma, T.P.; Koju, U.A.; Wang, J.; Nabil, M. Analyzing NPP Response of Different Rangeland Types to Climatic Parameters over Mongolia. *Agronomy* **2021**, *11*, 647. [CrossRef]
80. You, Y.; Wang, S.; Ma, Y.; Wang, X.; Liu, W. Improved Modeling of Gross Primary Productivity of Alpine Grasslands on the Tibetan Plateau Using the Biome-BGC Model. *Remote Sens.* **2019**, *11*, 1287. [CrossRef]
81. Biudes, M.S.; Vourlitis, G.L.; Velasque, M.C.S.; Machado, N.G.; Danelichen, V.H.d.M.; Pavão, V.M.; Arruda, P.H.Z.; Nogueira, J.d.S. Gross primary productivity of Brazilian Savanna (Cerrado) estimated by different remote sensing-based models. *Agric. For. Meteorol.* **2021**, *307*, 108456. [CrossRef]

82. Irisarri, J.G.N.; Texeira, M.; Oesterheld, M.; Veron, S.R.; Della Nave, F.; Paruelo, J.M. Discriminating the biophysical signal from human-induced effects on long-term primary production dynamics. The case of Patagonia. *Glob. Chang. Biol.* **2021**, *27*, 4381–4391. [CrossRef] [PubMed]
83. Yu, R. An improved estimation of net primary productivity of grassland in the Qinghai-Tibet region using light use efficiency with vegetation photosynthesis model. *Ecol. Model.* **2020**, *431*, 109121. [CrossRef]
84. Blanco, L.J.; Paruelo, J.M.; Oesterheld, M.; Agüero, W.D. Radiation use efficiency of the herbaceous layer of dry Chaco shrublands and woodlands: Spatial and temporal patterns. *Appl. Veg. Sci.* **2022**, *25*, e12653. [CrossRef]
85. Gaffney, R.; Porensky, L.M.; Gao, F.; Irisarri, J.G.; Durante, M.; Derner, J.D.; Augustine, D.J. Using APAR to Predict Aboveground Plant Productivity in semiarid Rangelands: Spatial and Temporal Relationships Differ. *Remote Sens.* **2018**, *10*, 1474. [CrossRef]
86. Liu, H.; Jin, Y.; Roche, L.M.; O'Geen, A.T.; Dahlgren, R.A. Understanding spatial variability of forage production in California grasslands: Delineating climate, topography and soil controls. *Environ. Res. Lett.* **2021**, *16*, 14043. [CrossRef]
87. Sakowska, K.; MacArthur, A.; Gianelle, D.; Dalponte, M.; Alberti, G.; Gioli, B.; Miglietta, F.; Pitacco, A.; Meggio, F.; Fava, F.; et al. Assessing Across-Scale Optical Diversity and Productivity Relationships in Grasslands of the Italian Alps. *Remote Sens.* **2019**, *11*, 614. [CrossRef]
88. Li, G.; Wang, J.; Wang, Y.; Wei, H.; Ochir, A.; Davaasuren, D.; Chonokhuu, S.; Nasanbat, E. Spatial and Temporal Variations in Grassland Production from 2006 to 2015 in Mongolia Along the China–Mongolia Railway. *Sustainability* **2019**, *11*, 2177. [CrossRef]
89. Zhang, T.; Yu, G.; Chen, Z.; Hu, Z.; Jiao, C.; Yang, M.; Fu, Z.; Zhang, W.; Han, L.; Fan, M.; et al. Patterns and controls of vegetation productivity and precipitation-use efficiency across Eurasian grasslands. *Sci. Total Environ.* **2020**, *741*, 140204. [CrossRef]
90. Xu, X.; Zhou, G.; Du, H.; Mao, F.; Xu, L.; Li, X.; Liu, L. Combined MODIS land surface temperature and greenness data for modeling vegetation phenology, physiology, and gross primary production in terrestrial ecosystems. *Sci. Total Environ.* **2020**, *726*, 137948. [CrossRef]
91. Reeves, M.C.; Hanberry, B.B.; Wilmer, H.; Kaplan, N.E.; Lauenroth, W.K. An Assessment of Production Trends on the Great Plains from 1984 to 2017. *Rangel. Ecol. Manag.* **2021**, *78*, 165–179. [CrossRef]
92. Dieguez, F.J.; Pereira, M. Uruguayan native grasslands net aerial primary production model and its application on safe stocking rate concept. *Ecol. Model.* **2020**, *430*, 109060. [CrossRef]
93. Meroni, M.; Fasbender, D.; Lopez-Lozano, R.; Migliavacca, M. Assimilation of Earth Observation Data Over Cropland and Grassland Sites into a Simple GPP Model. *Remote Sens.* **2019**, *11*, 749. [CrossRef]
94. Gómez Giménez, M.; de Jong, R.; Keller, A.; Rihm, B.; Schaepman, M.E. Studying the Influence of Nitrogen Deposition, Precipitation, Temperature, and Sunshine in Remotely Sensed Gross Primary Production Response in Switzerland. *Remote Sens.* **2019**, *11*, 1135. [CrossRef]
95. Scurlock, J.M.O.; Johnson, K.; Olson, R.J. Estimating net primary productivity from grassland biomass dynamics measurements. *Glob. Chang. Biol.* **2002**, *8*, 736–753. [CrossRef]
96. Xu, D.; Pu, Y.; Guo, X. A Semi-Automated Method to Extract Green and Non-Photosynthetic Vegetation Cover from RGB Images in Mixed Grasslands. *Sensors* **2020**, *20*, 6870. [CrossRef]
97. Kim, J.; Kang, S.; Seo, B.; Narantsetseg, A.; Han, Y. Estimating fractional green vegetation cover of Mongolian grasslands using digital camera images and MODIS satellite vegetation indices. *GIScience Remote Sens.* **2019**, *57*, 49–59. [CrossRef]
98. Zhang, S.; Chen, H.; Fu, Y.; Niu, H.; Yang, Y.; Zhang, B. Fractional Vegetation Cover Estimation of Different Vegetation Types in the Qaidam Basin. *Sustainability* **2019**, *11*, 864. [CrossRef]
99. He, Y.; Yang, J.; Guo, X. Green Vegetation Cover Dynamics in a Heterogeneous Grassland: Spectral Unmixing of Landsat Time Series from 1999 to 2014. *Remote Sens.* **2020**, *12*, 3826. [CrossRef]
100. Vermeulen, L.M.; Munch, Z.; Palmer, A. Fractional vegetation cover estimation in southern African rangelands using spectral mixture analysis and Google Earth Engine. *Comput. Electron. Agric.* **2021**, *182*, 105980. [CrossRef]
101. Jansen, V.; Kolden, C.; Schmalz, H. The Development of Near Real-Time Biomass and Cover Estimates for Adaptive Rangeland Management Using Landsat 7 and Landsat 8 Surface Reflectance Products. *Remote Sens.* **2018**, *10*, 1057. [CrossRef]
102. Meng, B.; Gao, J.; Liang, T.; Cui, X.; Ge, J.; Yin, J.; Feng, Q.; Xie, H. Modeling of Alpine Grassland Cover Based on Unmanned Aerial Vehicle Technology and Multi-Factor Methods: A Case Study in the East of Tibetan Plateau, China. *Remote Sens.* **2018**, *10*, 320. [CrossRef]
103. Ge, J.; Meng, B.; Liang, T.; Feng, Q.; Gao, J.; Yang, S.; Huang, X.; Xie, H. Modeling alpine grassland cover based on MODIS data and support vector machine regression in the headwater region of the Huanghe River, China. *Remote Sens. Environ.* **2018**, *218*, 162–173. [CrossRef]
104. Gao, X.; Dong, S.; Li, S.; Xu, Y.; Liu, S.; Zhao, H.; Yeomans, J.; Li, Y.; Shen, H.; Wu, S.; et al. Using the random forest model and validated MODIS with the field spectrometer measurement promote the accuracy of estimating aboveground biomass and coverage of alpine grasslands on the Qinghai-Tibetan Plateau. *Ecol. Indic.* **2020**, *112*, 106114. [CrossRef]
105. Lin, X.; Chen, J.; Lou, P.; Yi, S.; Qin, Y.; You, H.; Han, X. Improving the estimation of alpine grassland fractional vegetation cover using optimized algorithms and multi-dimensional features. *Plant Methods* **2021**, *17*, 96. [CrossRef]
106. Liu, X.; Feng, S.; Liu, H.; Ji, J. Patterns and determinants of woody encroachment in the eastern Eurasian steppe. *Land Degrad. Dev.* **2021**, *32*, 3536–3549. [CrossRef]
107. Yang, F.; He, F.; Li, S.; Li, M. Exploring Spatiotemporal Pattern of Grassland Cover in Western China from 1661 to 1996. *Int. J. Environ. Res Public Health* **2019**, *16*, 3160. [CrossRef]

108. Yang, F.; He, F.; Li, S. Spatially Explicit Reconstruction of Anthropogenic Grassland Cover Change in China from 1700 to 2000. *Land* **2020**, *9*, 270. [CrossRef]
109. Chai, G.; Wang, J.; Wang, G.; Kang, L.; Wu, M.; Wang, Z. Estimating fractional cover of non-photosynthetic vegetation in a typical grassland area of northern China based on Moderate Resolution Imaging Spectroradiometer (MODIS) image data. *Int. J. Remote Sens.* **2019**, *40*, 8793–8810. [CrossRef]
110. Yu, X.; Guo, Q.; Chen, Q.; Guo, X. Discrimination of Senescent Vegetation Cover from Landsat-8 OLI Imagery by Spectral Unmixing in the Northern Mixed Grasslands. *Can. J. Remote Sens.* **2019**, *45*, 192–208. [CrossRef]
111. Chai, G.; Wang, J.; Wu, M.; Li, G.; Zhang, L.; Wang, Z. Mapping the fractional cover of non-photosynthetic vegetation and its spatiotemporal variations in the Xilingol grassland using MODIS imagery (2000–2019). *Geocarto Int.* **2020**, 1–17. [CrossRef]
112. Pu, J.; Yan, K.; Zhou, G.; Lei, Y.; Zhu, Y.; Guo, D.; Li, H.; Xu, L.; Knyazikhin, Y.; Myneni, R.B. Evaluation of the MODIS LAI/FPAR Algorithm Based on 3D-RTM Simulations: A Case Study of Grassland. *Remote Sens.* **2020**, *12*, 3391. [CrossRef]
113. Imran, H.A.; Gianelle, D.; Rocchini, D.; Dalponte, M.; Martín, M.P.; Sakowska, K.; Wohlfahrt, G.; Vescovo, L. VIS-NIR, Red-Edge and NIR-Shoulder Based Normalized Vegetation Indices Response to Co-Varying Leaf and Canopy Structural Traits in Heterogeneous Grasslands. *Remote Sens.* **2020**, *12*, 2254. [CrossRef]
114. Punalekar, S.M.; Verhoef, A.; Quaife, T.L.; Humphries, D.; Bermingham, L.; Reynolds, C.K. Application of Sentinel-2A data for pasture biomass monitoring using a physically based radiative transfer model. *Remote Sens. Environ.* **2018**, *218*, 207–220. [CrossRef]
115. Pacheco-Labrador, J.; Perez-Priego, O.; El-Madany, T.S.; Julitta, T.; Rossini, M.; Guan, J.; Moreno, G.; Carvalhais, N.; Martín, M.P.; Gonzalez-Cascon, R.; et al. Multiple-constraint inversion of SCOPE. Evaluating the potential of GPP and SIF for the retrieval of plant functional traits. *Remote Sens. Environ.* **2019**, *234*, 111362. [CrossRef]
116. Klingler, A.; Schaumberger, A.; Vuolo, F.; Kalmár, L.B.; Pötsch, E.M. Comparison of Direct and Indirect Determination of Leaf Area Index in Permanent Grassland. *PFG J. Photogramm. Remote Sens. Geoinf. Sci.* **2020**, *88*, 369–378. [CrossRef]
117. Lu, B.; He, Y. Leaf Area Index Estimation in a Heterogeneous Grassland Using Optical, SAR, and DEM Data. *Can. J. Remote Sens.* **2019**, *45*, 618–633. [CrossRef]
118. Schwieder, M.; Buddeberg, M.; Kowalski, K.; Pfoch, K.; Bartsch, J.; Bach, H.; Pickert, J.; Hostert, P. Estimating Grassland Parameters from Sentinel-2: A Model Comparison Study. *PFG J. Photogramm. Remote Sens. Geoinf. Sci.* **2020**, *88*, 379–390. [CrossRef]
119. Zhou, H.; Wang, C.; Zhang, G.; Xue, H.; Wang, J.; Wan, H. Generating a Spatio-Temporal Complete 30 m Leaf Area Index from Field and Remote Sensing Data. *Remote Sens.* **2020**, *12*, 2394. [CrossRef]
120. Danner, M.; Berger, K.; Wocher, M.; Mauser, W.; Hank, T. Efficient RTM-based training of machine learning regression algorithms to quantify biophysical & biochemical traits of agricultural crops. *ISPRS J. Photogramm. Remote Sens.* **2021**, *173*, 278–296.
121. Reiche, M.; Funk, R.; Zhang, Z.D.; Hoffmann, C.; Reiche, J.; Wehrhan, M.; Li, Y.; Sommer, M. Application of satellite remote sensing for mapping wind erosion risk and dust emission-deposition in Inner Mongolia grassland, China. *Grassl. Sci.* **2012**, *58*, 8–19. [CrossRef]
122. Li, S.; Yan, C.Z.; Wang, T.; Du, H.Q. Monitoring grassland reclamation in the Mu Us Desert using remote sensing from 2010 to 2015. *Environ. Earth Sci.* **2019**, *78*, 311. [CrossRef]
123. Li, X.; Wang, H.; Li, X.; Tang, Z.; Liu, H. Identifying Degraded Grass Species in Inner Mongolia Based on Measured Hyperspectral Data. *IEEE J. Sel. Top. Appl. Earth Obs. Remote Sens.* **2020**, *12*, 1–15. [CrossRef]
124. Pi, W.; Du, J.; Bi, Y.; Gao, X.; Zhu, X. 3D-CNN based UAV hyperspectral imagery for grassland degradation indicator ground object classification research. *Ecol. Inform.* **2021**, *62*, 101278. [CrossRef]
125. Sternberg, T.; Tsolmon, R.; Middleton, N.; Thomas, D. Tracking desertification on the Mongolian steppe through NDVI and field-survey data. *Int. J. Digit. Earth* **2011**, *4*, 50–64. [CrossRef]
126. Wiesmair, M.; Feilhauer, H.; Magiera, A.; Otte, A.; Waldhardt, R. Estimating Vegetation Cover from High-Resolution Satellite Data to Assess Grassland Degradation in the Georgian Caucasus. *Mt. Res. Dev.* **2016**, *36*, 56–65. [CrossRef]
127. Li, J.; Yang, X.; Jin, Y.; Yang, Z.; Huang, W.; Zhao, L.; Gao, T.; Yu, H.; Ma, H.; Qin, Z.; et al. Monitoring and analysis of grassland desertification dynamics using Landsat images in Ningxia, China. *Remote Sens. Environ.* **2013**, *138*, 19–26. [CrossRef]
128. Xu, B.; Li, J.Y.; Jin, Y.X.; Wang, Z.L.; Qin, Z.H.; Wu, M.Q.; Wang, D.L.; Zhang, J.; Ma, H.L.; Yang, X.C. Temporal and spatial variations of grassland desertification monitoring in Tibet of China. *Int. J. Remote Sens.* **2015**, *36*, 5150–5164. [CrossRef]
129. Wang, Z.; Zhang, Y.; Yang, Y.; Zhou, W.; Gang, C.; Zhang, Y.; Li, J.; An, R.; Wang, K.; Odeh, I.; et al. Quantitative assess the driving forces on the grassland degradation in the Qinghai–Tibet Plateau, in China. *Ecol. Inform.* **2016**, *33*, 32–44. [CrossRef]
130. Zhumanova, M.; Mönnig, C.; Hergarten, C.; Darr, D.; Wrage-Mönnig, N. Assessment of vegetation degradation in mountainous pastures of the Western Tien-Shan, Kyrgyzstan, using eMODIS NDVI. *Ecol. Indic.* **2018**, *95*, 527–543. [CrossRef]
131. Han, W.; Lu, H.; Liu, G.; Wang, J.; Su, X. Quantifying Degradation Classifications on Alpine Grassland in the Lhasa River Basin, Qinghai-Tibetan Plateau. *Sustainability* **2019**, *11*, 7067. [CrossRef]
132. Lyu, X.; Li, X.B.; Gong, J.R.; Wang, H.; Dang, D.L.; Dou, H.S.; Li, S.K.; Liu, S.Y. Comprehensive Grassland Degradation Monitoring by Remote Sensing in Xilinhot, Inner Mongolia, China. *Sustainability* **2020**, *12*, 3682. [CrossRef]
133. Yang, Y.L.; Wang, J.L.; Chen, Y.; Cheng, F.; Liu, G.J.; He, Z.H. Remote-Sensing Monitoring of Grassland Degradation Based on the GDI in Shangri-La, China. *Remote Sens.* **2019**, *11*, 3030. [CrossRef]

134. Guo, B.; Zang, W.; Han, B.; Yang, F.; Luo, W.; He, T.; Fan, Y.; Yang, X.; Chen, S. Dynamic monitoring of desertification in Naiman Banner based on feature space models with typical surface parameters derived from LANDSAT images. *Land Degrad. Dev.* **2020**, *31*, 1573–1592. [CrossRef]
135. Qian, K.; Yuan, Q.Z.; Han, J.C.; Leng, R.; Wang, Y.S.; Zhu, K.H.; Lin, S.; Ren, P. A remote sensing monitoring method for alpine grasslands desertification in the eastern Qinghai-Tibetan Plateau. *J. Mt. Sci.* **2020**, *17*, 1423–1437.
136. Ma, Q.; Chai, L.; Hou, F.; Chang, S.; Ma, Y.; Tsunekawa, A.; Cheng, Y. Quantifying Grazing Intensity Using Remote Sensing in Alpine Meadows on Qinghai-Tibetan Plateau. *Sustainability* **2019**, *11*, 417. [CrossRef]
137. Li, F.; Zheng, J.; Wang, H.; Luo, J.; Zhao, Y.; Zhao, R. Mapping grazing intensity using remote sensing in the Xilingol steppe region, Inner Mongolia, China. *Remote Sens. Lett.* **2016**, *7*, 328–337. [CrossRef]
138. Hall, K.; Johansson, L.J.; Sykes, M.T.; Reitalu, T.; Larsson, K.; Prentice, H.C. Inventorying management status and plant species richness in semi-natural grasslands using high spatial resolution imagery. *Appl. Veg. Sci.* **2010**, *13*, 221–233. [CrossRef]
139. Yang, X.; Guo, X. Investigating vegetation biophysical and spectral parameters for detecting light to moderate grazing effects: A case study in mixed grass prairie. *Cent. Eur. J. Geosci.* **2011**, *3*, 336. [CrossRef]
140. Yu, R.; Evans, A.J.; Malleson, N. Quantifying grazing patterns using a new growth function based on MODIS Leaf Area Index. *Remote Sens. Environ.* **2018**, *209*, 181–194. [CrossRef]
141. Feng, X.M.; Zhao, Y.S. Grazing intensity monitoring in Northern China steppe: Integrating CENTURY model and MODIS data. *Ecol. Indic.* **2011**, *11*, 175–182. [CrossRef]
142. Jansen, V.S.; Kolden, C.A.; Taylor, R.V.; Newingham, B.A. Quantifying livestock effects on bunchgrass vegetation with Landsat ETM+ data across a single growing season. *Int. J. Remote Sens.* **2015**, *37*, 150–175. [CrossRef]
143. Li, F.; Bai, Y.; Wan, H.; Zheng, J.; Luo, J.; Zhao, D.; Liu, P. Quantifying Grazing Intensity in China Using High Temporal Resolution MODIS Data. *IEEE J. Sel. Top. Appl. Earth Obs. Remote Sens.* **2017**, *10*, 515–523. [CrossRef]
144. Sha, Z.; Brown, D.G.; Xie, Y.; Welsh, W.F.; Bai, Y. Response of spectral vegetation indices to a stocking rate experiment in Inner Mongolia, China. *Remote Sens. Lett.* **2014**, *5*, 912–921. [CrossRef]
145. Lei, G.; Li, A.; Zhang, Z.; Bian, J.; Hu, G.; Wang, C.; Nan, X.; Wang, J.; Tan, J.; Liao, X. The Quantitative Estimation of Grazing Intensity on the Zoige Plateau Based on the Space-Air-Ground Integrated Monitoring Technology. *Remote Sens.* **2020**, *12*, 1399. [CrossRef]
146. Gimenez, M.G.; de Jong, R.; Della Peruta, R.; Keller, A.; Schaepman, M.E. Determination of grassland use intensity based on multi-temporal remote sensing data and ecological indicators. *Remote Sens. Environ.* **2017**, *198*, 126–139. [CrossRef]
147. Franke, J.; Keuck, V.; Siegert, F. Assessment of grassland use intensity by remote sensing to support conservation schemes. *J. Nat. Conserv.* **2012**, *20*, 125–134. [CrossRef]
148. Li, F.; Zhao, Y.; Zheng, J.; Luo, J.; Zhang, X. Monitoring grazing intensity: An experiment with canopy spectra applied to satellite remote sensing. *J. Appl. Remote Sens.* **2016**, *10*, 026032. [CrossRef]
149. Zheng, J.; Li, F.; Du, X. Using Red Edge Position Shift to Monitor Grassland Grazing Intensity in Inner Mongolia. *J. Indian Soc. Remote Sens.* **2017**, *46*, 81–88. [CrossRef]
150. Dara, A.; Baumann, M.; Freitag, M.; Hölzel, N.; Hostert, P.; Kamp, J.; Müller, D.; Prishchepov, A.V.; Kuemmerle, T. Annual Landsat time series reveal post-Soviet changes in grazing pressure. *Remote Sens. Environ.* **2020**, *239*, 111667. [CrossRef]
151. Dusseux, P.; Vertes, F.; Corpetti, T.; Corgne, S.; Hubert-Moy, L. Agricultural practices in grasslands detected by spatial remote sensing. *Environ. Monit. Assess.* **2014**, *186*, 8249–8265. [CrossRef]
152. Asam, S.; Klein, D.; Dech, S. Estimation of grassland use intensities based on high spatial resolution LAI time series. *Int. Arch. Photogramm. Remote. Sens. Spat. Inf. Sci.* **2015**, *XL-7/W3*, 285–291. [CrossRef]
153. Estel, S.; Mader, S.; Levers, C.; Verburg, P.H.; Baumann, M.; Kuemmerle, T. Combining satellite data and agricultural statistics to map grassland management intensity in Europe. *Environ. Res. Lett.* **2018**, *13*, 74020. [CrossRef]
154. Griffiths, P.; Nendel, C.; Pickert, J.; Hostert, P. Towards national-scale characterization of grassland use intensity from integrated Sentinel-2 and Landsat time series. *Remote Sens. Environ.* **2020**, *238*, 111124. [CrossRef]
155. Stumpf, F.; Schneider, M.K.; Keller, A.; Mayr, A.; Rentschler, T.; Meuli, R.G.; Schaepman, M.; Liebisch, F. Spatial monitoring of grassland management using multi-temporal satellite imagery. *Ecol. Indic.* **2020**, *113*, 106201. [CrossRef]
156. Griffiths, P.; Nendel, C.; Hostert, P. Intra-annual reflectance composites from Sentinel-2 and Landsat for national-scale crop and land cover mapping. *Remote Sens. Environ.* **2019**, *220*, 135–151. [CrossRef]
157. Martin, D.; Chen, T.; Nichols, D.; Bessell, R.; Kidnie, S.; Alexander, J. Integrating ground and satellite-based observations to determine the degree of grassland curing. *Int. J. Wildland Fire* **2015**, *24*, 329–339. [CrossRef]
158. Chaivaranont, W.; Evans, J.P.; Liu, Y.Y.; Sharples, J.J. Estimating grassland curing with remotely sensed data. *Nat. Hazards Earth Syst. Sci.* **2018**, *18*, 1535–1554. [CrossRef]
159. Li, S. Analysis of Landsat 8 detection of the interannual variability of grassland curing in Greater Melbourne, Australia. *Int. J. Digit. Earth* **2020**, *13*, 1321–1338. [CrossRef]
160. Li, S. Inter-satellite variability of grassland curing maps produced by different satellite sensors—Victoria, Australia. *Int. J. Digit. Earth* **2021**, *14*, 899–920. [CrossRef]
161. Wang, L.; Zhou, Y.; Zhou, W.; Wang, S. Fire danger assessment with remote sensing: A case study in Northern China. *Nat. Hazards* **2012**, *65*, 819–834. [CrossRef]

162. Bian, H.; Zhang, H.; Zhou, D.; Xu, J.; Zhang, Z. Integrating models to evaluate and map grassland fire risk zones in Hulunbuir of Inner Mongolia, China. *Fire Saf. J.* **2013**, *61*, 207–216. [CrossRef]
163. Sesnie, S.E.; Eagleston, H.; Johnson, L.; Yurcich, E. In-Situ and Remote Sensing Platforms for Mapping Fine-Fuels and Fuel-Types in Sonoran Semi-Desert Grasslands. *Remote Sens.* **2018**, *10*, 1358. [CrossRef]
164. Jurdao, S.; Chuvieco, E.; Arevalillo, J.M. Modelling Fire Ignition Probability from Satellite Estimates of Live Fuel Moisture Content. *Fire Ecol.* **2012**, *8*, 77–97. [CrossRef]
165. Arganaraz, J.P.; Landi, M.A.; Bravo, S.J.; Gavier-Pizarro, G.I.; Scavuzzo, C.M.; Bellis, L.M. Estimation of Live Fuel Moisture Content From MODIS Images for Fire Danger Assessment in Southern Gran Chaco. *IEEE J. Sel. Top. Appl. Earth Obs. Remote Sens.* **2016**, *9*, 5339–5349. [CrossRef]
166. Luo, K.; Quan, X.; He, B.; Yebra, M. Effects of Live Fuel Moisture Content on Wildfire Occurrence in Fire-Prone Regions over Southwest China. *Forests* **2019**, *10*, 887. [CrossRef]
167. Yebra, M.; Quan, X.; Riaño, D.; Rozas Larraondo, P.; van Dijk, A.I.J.M.; Cary, G.J. A fuel moisture content and flammability monitoring methodology for continental Australia based on optical remote sensing. *Remote Sens. Environ.* **2018**, *212*, 260–272. [CrossRef]
168. Dubinin, M.; Potapov, P.; Lushchekina, A.; Radeloff, V.C. Reconstructing long time series of burned areas in arid grasslands of southern Russia by satellite remote sensing. *Remote Sens. Environ.* **2010**, *114*, 1638–1648. [CrossRef]
169. Pereira Junior, A.C.; Oliveira, S.L.; Pereira, J.M.; Turkman, M.A. Modelling fire frequency in a Cerrado savanna protected area. *PLoS ONE* **2014**, *9*, e102380. [CrossRef]
170. Cao, X.; Cui, X.; Yue, M.; Chen, J.; Tanikawa, H.; Ye, Y. Evaluation of wildfire propagation susceptibility in grasslands using burned areas and multivariate logistic regression. *Int. J. Remote Sens.* **2013**, *34*, 6679–6700. [CrossRef]
171. Li, Z.; Shi, H.; Vogelmann, J.E.; Hawbaker, T.J.; Peterson, B. Assessment of Fire Fuel Load Dynamics in Shrubland Ecosystems in the Western United States Using MODIS Products. *Remote Sens.* **2020**, *12*, 1911. [CrossRef]
172. Justice, C.; Giglio, L.; Korontzi, S.; Owens, J.; Morisette, J.; Roy, D.; Descloitres, J.; Alleaume, S.; Petitcolin, F.; Kaufman, Y. The MODIS fire products. *Remote Sens. Environ.* **2002**, *83*, 244–262. [CrossRef]
173. Alvarado, S.T.; Andela, N.; Silva, T.S.F.; Archibald, S.; Poulter, B. Thresholds of fire response to moisture and fuel load differ between tropical savannas and grasslands across continents. *Glob. Ecol. Biogeogr.* **2019**, *29*, 331–344. [CrossRef]
174. Cai, L.; Wang, M. Is the RdNBR a better estimator of wildfire burn severity than the dNBR? A discussion and case study in southeast China. *Geocarto Int.* **2020**, *37*, 758–772. [CrossRef]
175. Dara, A.; Baumann, M.; Hölzel, N.; Hostert, P.; Kamp, J.; Müller, D.; Ullrich, B.; Kuemmerle, T. Post-Soviet Land-Use Change Affected Fire Regimes on the Eurasian Steppes. *Ecosystems* **2019**, *23*, 943–956. [CrossRef]
176. Liu, M.; Zhao, J.; Guo, X.; Zhang, Z.; Tan, G.; Yang, J. Study on Climate and Grassland Fire in HulunBuir, Inner Mongolia Autonomous Region, China. *Sensors* **2017**, *17*, 616. [CrossRef]
177. Verhoeven, E.M.; Murray, B.R.; Dickman, C.R.; Wardle, G.M.; Greenville, A.C. Fire and rain are one: Extreme rainfall events predict wildfire extent in an arid grassland. *Int. J. Wildland Fire* **2020**, *29*, 702–711. [CrossRef]
178. Adagbasa, E.G.; Adelabu, S.A.; Okello, T.W. Development of post-fire vegetation response-ability model in grassland mountainous ecosystem using GIS and remote sensing. *ISPRS J. Photogramm. Remote Sens.* **2020**, *164*, 173–183. [CrossRef]
179. Steiner, J.L.; Wetter, J.; Robertson, S.; Teet, S.; Wang, J.; Wu, X.; Zhou, Y.; Brown, D.; Xiao, X. Grassland Wildfires in the Southern Great Plains: Monitoring Ecological Impacts and Recovery. *Remote Sens.* **2020**, *12*, 619. [CrossRef]
180. Han, A.; Qing, S.; Bao, Y.; Na, L.; Bao, Y.; Liu, X.; Zhang, J.; Wang, C. Short-Term Effects of Fire Severity on Vegetation Based on Sentinel-2 Satellite Data. *Sustainability* **2021**, *13*, 432. [CrossRef]
181. Ratajczak, Z.; Briggs, J.M.; Goodin, D.G.; Luo, L.; Mohler, R.L.; Nippert, J.B.; Obermeyer, B. Assessing the Potential for Transitions from Tallgrass Prairie to Woodlands: Are We Operating Beyond Critical Fire Thresholds? *Rangel. Ecol. Manag.* **2016**, *69*, 280–287. [CrossRef]
182. Wei, W.; Zhang, J.; Zhou, L.; Xie, B.; Zhou, J.; Li, C. Comparative evaluation of drought indices for monitoring drought based on remote sensing data. *Environ. Sci. Pollut. Res.* **2021**, *28*, 20408–20425. [CrossRef]
183. Muthumanickam, D.; Kannan, P.; Kumaraperumal, R.; Natarajan, S.; Sivasamy, R.; Poongodi, C. Drought assessment and monitoring through remote sensing and GIS in western tracts of Tamil Nadu, India. *Int. J. Remote Sens.* **2011**, *32*, 5157–5176. [CrossRef]
184. Cao, X.; Feng, Y.; Shi, Z. Spatio-temporal Variations in Drought with Remote Sensing from the Mongolian Plateau During 1982–2018. *Chin. Geogr. Sci.* **2020**, *30*, 1081–1094. [CrossRef]
185. Zhang, A.; Jia, G. Monitoring meteorological drought in semiarid regions using multi-sensor microwave remote sensing data. *Remote Sens. Environ.* **2013**, *134*, 12–23. [CrossRef]
186. Hermanns, F.; Pohl, F.; Rebmann, C.; Schulz, G.; Werban, U.; Lausch, A. Inferring Grassland Drought Stress with Unsupervised Learning from Airborne Hyperspectral VNIR Imagery. *Remote Sens.* **2021**, *13*, 1885. [CrossRef]
187. Chang, S.; Wu, B.; Yan, N.; Davdai, B.; Nasanbat, E. Suitability Assessment of Satellite-Derived Drought Indices for Mongolian Grassland. *Remote Sens.* **2017**, *9*, 650. [CrossRef]
188. Liu, G.X.; Yi, Z.; Yu, F.M.; Jiang, C.L. Study on Effect of Drought Based on Time Series on Grassland Vegetation in Eastern Inner Mongolia. *Adv. Mater. Res.* **2012**, *518*, 5306–5315. [CrossRef]

189. Li, R.; Wang, J.; Zhao, T.; Shi, J. Index-based evaluation of vegetation response to meteorological drought in Northern China. *Nat. Hazards* **2016**, *84*, 2179–2193. [CrossRef]
190. Liu, S.; Zhang, Y.; Cheng, F.; Hou, X.; Zhao, S. Response of Grassland Degradation to Drought at Different Time-Scales in Qinghai Province: Spatio-Temporal Characteristics, Correlation, and Implications. *Remote Sens.* **2017**, *9*, 1329. [CrossRef]
191. Villarreal, M.L.; Norman, L.M.; Buckley, S.; Wallace, C.S.A.; Coe, M.A. Multi-index time series monitoring of drought and fire effects on desert grasslands. *Remote Sens. Environ.* **2016**, *183*, 186–197. [CrossRef]
192. Ding, J.; Yang, T.; Zhao, Y.; Liu, D.; Wang, X.; Yao, Y.; Peng, S.; Wang, T.; Piao, S. Increasingly Important Role of Atmospheric Aridity on Tibetan Alpine Grasslands. *Geophys. Res. Lett.* **2018**, *45*, 2852–2859. [CrossRef]
193. Chen, N.; Zhang, Y.; Zu, J.; Zhu, J.; Zhang, T.; Huang, K.; Cong, N.; Wang, Z.; Li, J.; Zheng, Z.; et al. The compensation effects of post-drought regrowth on earlier drought loss across the tibetan plateau grasslands. *Agric. For. Meteorol.* **2020**, *281*, 107822. [CrossRef]
194. Poděbradská, M.; Wylie, B.K.; Hayes, M.J.; Wardlow, B.D.; Bathke, D.J.; Bliss, N.B.; Dahal, D. Monitoring Drought Impact on Annual Forage Production in semiarid Grasslands: A Case Study of Nebraska Sandhills. *Remote Sens.* **2019**, *11*, 2106. [CrossRef]
195. van Rooijen, N.M.; de Keersmaecker, W.; Ozinga, W.A.; Coppin, P.; Hennekens, S.M.; Schaminée, J.H.J.; Somers, B.; Honnay, O. Plant Species Diversity Mediates Ecosystem Stability of Natural Dune Grasslands in Response to Drought. *Ecosystems* **2015**, *18*, 1383–1394. [CrossRef]
196. Cui, T.; Martz, L.; Guo, X. Grassland Phenology Response to Drought in the Canadian Prairies. *Remote Sens.* **2017**, *9*, 1258. [CrossRef]
197. Cao, X.; Feng, Y.; Wang, J. Remote sensing monitoring the spatio-temporal changes of aridification in the Mongolian Plateau based on the general Ts-NDVI space, 1981–2012. *J. Earth Syst. Sci.* **2017**, *126*, 58. [CrossRef]
198. Han, D.; Wang, G.; Liu, T.; Xue, B.L.; Kuczera, G.; Xu, X. Hydroclimatic response of evapotranspiration partitioning to prolonged droughts in semiarid grassland. *J. Hydrol.* **2018**, *563*, 766–777. [CrossRef]
199. Wang, W.; Liang, T.; Huang, X.; Feng, Q.; Xie, H.; Liu, X.; Chen, M.; Wang, X. Early warning of snow-caused disasters in pastoral areas on the Tibetan Plateau. *Nat. Hazards Earth Syst. Sci.* **2013**, *13*, 1411–1425. [CrossRef]
200. Yang, W.; Qi, W. Spatial-Temporal Dynamic Monitoring of Vegetation Recovery After the Wenchuan Earthquake. *IEEE J. Sel. Top. Appl. Earth Obs. Remote Sens.* **2017**, *10*, 868–876. [CrossRef]
201. Hu, T.; Smith, R. The Impact of Hurricane Maria on the Vegetation of Dominica and Puerto Rico Using Multispectral Remote Sensing. *Remote Sens.* **2018**, *10*, 827. [CrossRef]
202. Sakowska, K.; Vescovo, L.; Marcolla, B.; Juszczak, R.; Olejnik, J.; Gianelle, D. Monitoring of carbon dioxide fluxes in a subalpine grassland ecosystem of the Italian Alps using a multispectral sensor. *Biogeosciences* **2014**, *11*, 4695–4712. [CrossRef]
203. Umair, M.; Kim, D.; Ray, R.L.; Choi, M. Evaluation of atmospheric and terrestrial effects in the carbon cycle for forest and grassland ecosystems using a remote sensing and modeling approach. *Agric. For. Meteorol.* **2020**, *295*, 108187. [CrossRef]
204. Chen, Z.; Yu, G. Spatial variations and controls of carbon use efficiency in China's terrestrial ecosystems. *Sci. Rep.* **2019**, *9*, 19516. [CrossRef]
205. Yan, W.; Hu, Z.; Zhao, Y.; Zhang, X.; Fan, Y.; Shi, P.; He, Y.; Yu, G.; Li, Y. Modeling net ecosystem carbon exchange of alpine grasslands with a satellite-driven model. *PLoS ONE* **2015**, *10*, e0122486. [CrossRef]
206. Berberoglu, S.; Donmez, C.; Evrendilek, F. Coupling of remote sensing, field campaign, and mechanistic and empirical modeling to monitor spatiotemporal carbon dynamics of a Mediterranean watershed in a changing regional climate. *Environ. Monit. Assess.* **2015**, *187*, 179. [CrossRef]
207. Dai, E.; Huang, Y.; Wu, Z.; Zhao, D. Analysis of spatio-temporal features of a carbon source/sink and its relationship to climatic factors in the Inner Mongolia grassland ecosystem. *J. Geogr. Sci.* **2016**, *26*, 297–312. [CrossRef]
208. Nestola, E.; Calfapietra, C.; Emmerton, C.; Wong, C.; Thayer, D.; Gamon, J. Monitoring Grassland Seasonal Carbon Dynamics, by Integrating MODIS NDVI, Proximal Optical Sampling, and Eddy Covariance Measurements. *Remote Sens.* **2016**, *8*, 260. [CrossRef]
209. Noumonvi, K.; Ferlan, M.; Eler, K.; Alberti, G.; Peressotti, A.; Cerasoli, S. Estimation of Carbon Fluxes from Eddy Covariance Data and Satellite-Derived Vegetation Indices in a Karst Grassland (Podgorski Kras, Slovenia). *Remote Sens.* **2019**, *11*, 649. [CrossRef]
210. Delgado-Balbuena, J.; Arredondo, J.T.; Loescher, H.W.; Pineda-Martínez, L.F.; Carbajal, J.N.; Vargas, R. Seasonal Precipitation Legacy Effects Determine the Carbon Balance of a Semiarid Grassland. *J. Geophys. Res. Biogeosci.* **2019**, *124*, 987–1000. [CrossRef]
211. Kazar, S.A.; Warner, T.A. Assessment of carbon storage and biomass on minelands reclaimed to grassland environments using Landsat spectral indices. *J. Appl. Remote Sens.* **2013**, *7*, 073583. [CrossRef]
212. Xia, J.; Liu, S.; Liang, S.; Chen, Y.; Xu, W.; Yuan, W. Spatio-Temporal Patterns and Climate Variables Controlling of Biomass Carbon Stock of Global Grassland Ecosystems from 1982 to 2006. *Remote Sens.* **2014**, *6*, 1783–1802. [CrossRef]
213. Ding, L.; Li, Z.; Wang, X.; Yan, R.; Shen, B.; Chen, B.; Xin, X. Estimating Grassland Carbon Stocks in Hulunber China, Using Landsat8 Oli Imagery and Regression Kriging. *Sensors* **2019**, *19*, 5374. [CrossRef]
214. Dai, E.; Zhai, R.; Ge, Q.; Wu, X. Detecting the storage and change on topsoil organic carbon in grasslands of Inner Mongolia from 1980s to 2010s. *J. Geogr. Sci.* **2014**, *24*, 1035–1046. [CrossRef]
215. Guoqing, L.; Xiaobing, L.; Tao, Z.; Hong, W.; Ruihua, L.; Han, W.; Dandan, W. A Model for Simulating the Soil Organic Carbon Pool of Steppe Ecosystems. *Environ. Model. Assess.* **2015**, *21*, 339–355. [CrossRef]
216. Venter, Z.S.; Hawkins, H.J.; Cramer, M.D.; Mills, A.J. Mapping soil organic carbon stocks and trends with satellite-driven high resolution maps over South Africa. *Sci. Total Environ.* **2021**, *771*, 145384. [CrossRef] [PubMed]

217. Sabathier, R.; Singer, M.B.; Stella, J.C.; Roberts, D.A.; Caylor, K.K. Vegetation responses to climatic and geologic controls on water availability in southeastern Arizona. *Environ. Res. Lett.* **2021**, *16*, 064029. [CrossRef]
218. Liu, S.; Roberts, D.A.; Chadwick, O.A.; Still, C.J. Spectral responses to plant available soil moisture in a Californian grassland. *Int. J. Appl. Earth Obs. Geoinf.* **2012**, *19*, 31–44. [CrossRef]
219. Galvão, L.S.; dos Santos, J.R.; Roberts, D.A.; Breunig, F.M.; Toomey, M.; de Moura, Y.M. On intra-annual EVI variability in the dry season of tropical forest: A case study with MODIS and hyperspectral data. *Remote Sens. Environ.* **2011**, *115*, 2350–2359. [CrossRef]
220. Moura, Y.M.; Galvão, L.S.; dos Santos, J.R.; Roberts, D.A.; Breunig, F.M. Use of MISR/Terra data to study intra- and inter-annual EVI variations in the dry season of tropical forest. *Remote Sens. Environ.* **2012**, *127*, 260–270. [CrossRef]